

How irreversible are steady-state trajectories of a trapped active particle?

Lennart Dabelow¹, Stefano Bo² and Ralf Eichhorn³

¹Fakultät für Physik, Universität Bielefeld, 33615 Bielefeld, Germany

²Max-Planck-Institute for the Physics of Complex Systems, Nöthnitzerstr. 38, 01187 Dresden, Germany

³Nordita, Royal Institute of Technology and Stockholm University, Roslagstullsbacken 23, SE-106 91 Stockholm, Sweden

E-mail: ldabelow@physik.uni-bielefeld.de, stefabo@pks.mpg.de, ralf.eichhorn@nordita.org

Abstract. The defining feature of active particles is that they constantly propel themselves by locally converting chemical energy into directed motion. This active self-propulsion prevents them from equilibrating with their thermal environment (e.g., an aqueous solution), thus keeping them permanently out of equilibrium. Nevertheless, the spatial dynamics of active particles might share certain equilibrium features, in particular in the steady state. We here focus on the time-reversal symmetry of individual spatial trajectories as a distinct equilibrium characteristic. We investigate to what extent the steady-state trajectories of a trapped active particle obey or break this time-reversal symmetry. Within the framework of active Ornstein-Uhlenbeck particles we find that the steady-state trajectories in a harmonic potential fulfill path-wise time-reversal symmetry exactly, while this symmetry is typically broken in anharmonic potentials.

PACS numbers: 05.70.Ln, 05.40.-a, 05.20.-y

Contents

1	Introduction	3
2	Model	4
3	Path weights and irreversibility	5
4	Harmonic trap	7
4.1	Path probability ratio in the joint steady state	7
4.2	Path-wise reversibility	9
4.3	Remark on $d > 1$ dimensions	10

<i>How irreversible are steady-state trajectories of a trapped active particle?</i>	2
5 Double-well potential	11
5.1 First numerical experiments	12
5.2 Explaining irreversibility	13
5.3 Exploring irreversibility	15
5.3.1 Decreasing active correlation time at constant active diffusion. . .	15
5.3.2 Decreasing active correlation time at constant active velocity. . .	17
6 Quartic single-well potential	19
7 Conclusions	21
Appendix A Calculation of $\Gamma_{\text{HP}}(t, t')$	24
Appendix B Reversibility in the harmonic potential	25

1. Introduction

For ordinary, *passive* Brownian motion in a confining potential, the steady state is in thermal equilibrium with the surrounding heat bath. Accordingly, the steady-state dynamics is reversible, i.e. it is equally likely to observe a specific trajectory being traced out forward in time as to observe it being traced out in the reversed direction backward in time. This path-wise reversibility is ultimately connected to conservation of entropy. Along any trajectory, entropy production in the environment is exactly canceled by the entropy change in the system. These statements can be made mathematically precise by comparing path probability densities for the forward and backward dynamics [1–3].

For *active* Brownian motion [4–8], on the other hand, the active self-propulsion drive creates a perpetual non-equilibrium situation which persists even in the steady state in a confining potential. Typical systems we have in mind are active colloids or living bacteria in suspension [5, 6, 9], which are manipulated by optical tweezers [10]. The active particles are maintained out of equilibrium by the microscopic processes generating the active self-propulsion. The details behind these processes are, however, mostly irrelevant for the dynamical and collective behavior emerging on the scales of the size of the active particles. Moreover, they are often inaccessible in typical experimental setups. Current video microscopy technology is generally unable to map out the microscopic details of, e.g., the movement of flagella of a bacterium or to track the chemical reactions on the surface of a Janus-colloid, let alone to separate the induced active motion entirely from thermal fluctuations. Individual trajectories of particles (in the form of particle position as a function of time) are therefore the central physical observables in a typical experiment. The question then arises, in how far the irreversible non-equilibrium nature of the active self-propulsion is visible (or detectable) on the level of individual particle trajectories [11–16]. Answering this question contributes to the endeavor of developing a theoretical framework for the “thermodynamics of active matter” [17–31] as it helps to understand under which conditions the (collective) steady state of active matter emerging from self-propulsion appears to have equilibrium characteristics and under which conditions its non-equilibrium nature becomes apparent.

We here focus on the trajectory-wise (ir)reversibility as described in the beginning of the Introduction to assess how closely active steady-state dynamics resemble equilibrium. In order to exclude the possibility of activity-induced currents in the spatial coordinate as obvious signatures of non-equilibrium, we consider the simple situation of active Brownian motion in a time-independent one-dimensional confining potential with active driving which is unbiased in space and time. Since the microscopic mechanisms which generate the active self-propulsion are of no interest for our trajectory-based analysis, we adopt the common strategy to include self-propulsion as an effective force into the equations of motion for a Brownian particle [4, 6]. A particularly successful such model is the so-called active Ornstein-Uhlenbeck particle (AOUP) [32]. In the AOUP model the active force is represented by a stochastic Ornstein-Uhlenbeck process [33, 34], without including the matching damping kernel [35] such that the equilibrium

fluctuation-dissipation relation [36, 37] is not fulfilled. In that way, the AOUP is constantly driven out of thermal equilibrium by a fluctuating “self-propulsion” force with exponentially decaying correlations which represent the directional persistence typical for active self-propulsion. Due to its conceptual simplicity, the AOUP has become a quite popular and successful model for active Brownian motion [8, 10, 11, 21, 28, 31, 38–59].

We present the mathematical details of the AOUP model in the next Section. Then, in Section 3 we introduce the statistical weight of individual trajectories as our main quantity of interest in order to quantify irreversibility by comparing forward and backward paths. We study different “minimal” trapping potentials in Section 4 (harmonic trap), Section 5 (anharmonic double-well), and Section 6 (anharmonic single-well) with surprising findings concerning the (ir)reversibility of individual steady-state trajectories of the AOUP in the various traps. We conclude in Section 7 with a short summary and discussion.

2. Model

We study a single particle in one dimension, which is in contact with a thermal environment at temperature T and, additionally, is driven by active Ornstein-Uhlenbeck fluctuations. This so-called active Ornstein-Uhlenbeck particle (AOUP) is confined by an external potential $U(x)$ with $U(x) \rightarrow \infty$ as $|x| \rightarrow \infty$ (faster than logarithmically). The overdamped equation of motion reads

$$\dot{x}(t) = -\frac{1}{\gamma}U'(x(t)) + \sqrt{2D_a}\eta(t) + \sqrt{2D}\xi(t). \quad (1)$$

Here, $\xi(t)$ is a Gaussian white-noise process with $\langle \xi(t) \rangle = 0$ and $\langle \xi(t)\xi(t') \rangle = \delta(t - t')$. The thermal diffusion coefficient $D = k_B T / \gamma$ is related to temperature T and viscous friction γ via the fluctuation-dissipation relation (k_B is Boltzmann’s constant), indicating that the environment constitutes a thermal bath at equilibrium. The active fluctuations are described by the stationary Ornstein-Uhlenbeck process $\eta(t)$ satisfying

$$\dot{\eta}(t) = -\frac{1}{\tau_a}\eta(t) + \frac{1}{\tau_a}\zeta(t) \quad (2)$$

with another Gaussian white noise source $\zeta(t)$, which is independent of $\xi(t)$. Consequently, $\eta(t)$ is a Gaussian process with $\langle \eta(t) \rangle = 0$ and

$$\langle \eta(t)\eta(t') \rangle = \frac{1}{2\tau_a}e^{-|t-t'|/\tau_a}. \quad (3)$$

This model of the active fluctuations is not directly related to the operational details of the self-propulsion drive. The variable $\eta(t)$ rather provides an *effective*, bath-like description of the drive’s statistical properties. The actual observable quantities in a typical experiment are particle positions $x(t)$ as a function of time, i.e. AOUP trajectories $\bar{x} = \{x(t)\}_{t=0}^{\tau}$ starting at time $t = 0$ and ending at time $t = \tau$.

3. Path weights and irreversibility

Our central quantity of interest is the probability to observe a trajectory $\bar{x} = \{x(t)\}_{t=0}^\tau$ starting in x_0 at time $t = 0$. We calculate this so-called path weight $\mathbf{p}[\bar{x}]$ by considering the joint path weight $\mathbf{p}[\underline{x}, \underline{\eta}|x_0, \eta_0]$ for the combined trajectory $(\underline{x}, \underline{\eta}) = \{(x(t), \eta(t))\}_{t \geq 0}^\tau$ conditioned on a fixed starting configuration (x_0, η_0) , and integrating over all possible realizations of $\bar{\eta} = \eta_0 \cup \underline{\eta}$,

$$\mathbf{p}[\bar{x}] = \int \mathcal{D}\bar{\eta} \mathbf{p}[\underline{x}, \underline{\eta}|x_0, \eta_0] p_0(x_0, \eta_0), \quad (4)$$

where the joint distribution of initial configurations (x_0, η_0) is given by $p_0(x_0, \eta_0)$. Since the combined process $(\underline{x}, \underline{\eta})$ is Markovian, we can express its path weight via the standard Onsager-Machlup path integral [60–62]

$$\mathbf{p}[\underline{x}, \underline{\eta}|x_0, \eta_0] \propto \exp \left\{ - \int_0^\tau dt \left[\frac{(\dot{x}_t - v_t - \sqrt{2D_a} \eta_t)^2}{4D} + \frac{(\tau_a \dot{\eta}_t + \eta_t)^2}{2} + \frac{1}{2} \frac{\partial v_t}{\partial x} \right] \right\}, \quad (5)$$

where we introduce the shorthand notation $x_t \equiv x(t)$, $\eta_t \equiv \eta(t)$ and $v_t \equiv -U'(x(t))/\gamma$. Note that the integral in (5) has been derived using a mid-point discretization (Stratonovich convention), which we tacitly assume for all stochastic integrals in the following. This path weight is quadratic in the active driving $\eta(t)$, such that the functional integral $\int \mathcal{D}\bar{\eta}$ in (4) is a “Gaussian integral in function space” and can be performed analytically [13], provided that the initial distribution is Gaussian in η_0 too, because $\int \mathcal{D}\bar{\eta}$ includes the integral over the initial point η_0 .

Using the path weight $\mathbf{p}[\bar{x}]$, we can then assess the irreversibility of individual trajectories by comparing the probability $\mathbf{p}[\bar{x}]$ to observe a trajectory $\bar{x} = \{x(t)\}_{t=0}^\tau$ forward in time with the probability $\mathbf{p}[\tilde{\bar{x}}]$ to observe its time-reversed twin $\tilde{\bar{x}} = \{x(\tau - t)\}_{t=0}^\tau$ ‡. In fact, the log ratio of path probabilities

$$\Delta\Sigma[\bar{x}] = k_B \ln \frac{\mathbf{p}[\bar{x}]}{\mathbf{p}[\tilde{\bar{x}}]} \quad (6)$$

has been adopted as a natural measure to quantify the “breaking” of time-reversal symmetry, i.e. to quantify irreversibility [1, 2, 63]. By definition, the process appears reversible if $\Delta\Sigma[\bar{x}] = 0$, since then the forward and backward trajectories occur with identical probabilities. A positive value indicates that the trajectory \bar{x} is more likely to be observed than its time-reversed twin $\tilde{\bar{x}}$ and vice versa for a negative value. Its mean (averaged over all possible trajectories) provides a way to estimate the arrow of time on statistical grounds [64]. Physically, the log ratio of path probabilities (6) can be related to the entropy production in the thermal environment and the path-wise mutual information between particle trajectories and active fluctuations [13]. Without activity ($D_a = 0$), i.e. for passive particles, it coincides with the standard notion of total entropy production as defined in stochastic thermodynamics [2, 3].

‡ In the absence of time-dependent forces, which is the case in our current setting, the probability functional \mathbf{p} is the same for forward and backward processes. Only if there were a time-dependent experimental protocol for the external forces, we would need to reverse this protocol as well and would in general obtain a different functional $\tilde{\mathbf{p}}$.

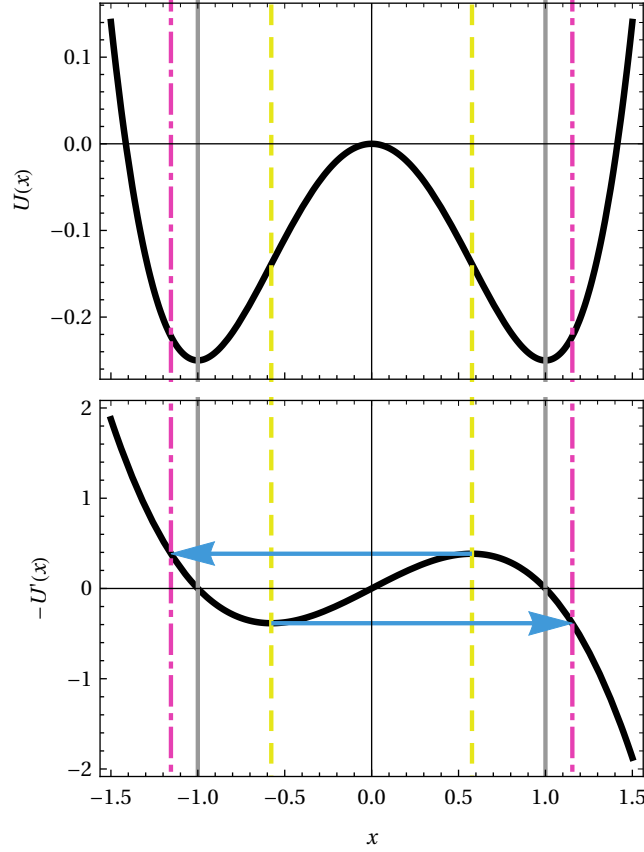


Figure 1. Anharmonic potential $U(x)$ from (7) for $k_4 = 1$ and $k_2 = -1$ (upper panel) and corresponding force $-U'(x)$ (lower panel). Potential minima are marked by solid gray lines. Inflection points are marked by dashed yellow lines. The corresponding conjugate points of equal force are marked by dash-dotted purple lines. The blue arrows illustrate the jumps in the high-persistence limit of large τ_a .

In the following we apply $\Delta\Sigma[\bar{x}]$ for assessing the reversible or irreversible character of steady-state trajectories of an AOUP trapped in a confining potential. It will turn out that the simplest trapping potentials to reveal essential irreversibility features are a quartic potential ($k_4 \geq 0$),

$$U(x) = \frac{k_4}{4}x^4 + \frac{k_2}{2}x^2, \quad (7)$$

and its various “special cases”, i.e. a harmonic trap ($k_4 = 0$ and $k_2 > 0$, Section 4), a double-well potential ($k_4 > 0$ and $k_2 < 0$, Section 5) and a quartic single-well potential ($k_4 > 0$ and $k_2 = 0$, Section 6). See Fig. 1 (upper panel) for an example of a quartic double-well potential with $k_2 = -1$ and $k_4 = 1$ in (7). We are interested in trajectories that start, remain and end in the steady state. However, in a typical initial setup (short) transients are often unavoidable, for instance, because the initial particle distribution did not yet relax within the potential or did not yet build up its steady-state correlations with the active fluctuations. The relative importance of these transients quickly diminishes over time and thus they are irrelevant for sufficiently long trajectories, i.e. longer than a few relaxation times within the potential and correlation

times of the active fluctuations. In other words, performing numerical experiments for long enough trajectories, the effect of short initial transients while approaching the joint steady state of x and η can be neglected.

4. Harmonic trap

In this Section, we consider the case $k_4 = 0$ and $k_2 > 0$ in (7). This case of a harmonic trap is interesting, because, by extending our method from [13], we can calculate $\Delta\Sigma[\bar{x}]$ analytically for an initial distribution $p_0(x_0, \eta_0)$ in (4) representing the joint steady state. We thus end up with a steady-state expression for $\Delta\Sigma[\bar{x}]$ that does not contain any of the above mentioned transients.

4.1. Path probability ratio in the joint steady state

The joint system with degrees of freedom $\mathbf{q} = (x, \eta)$ is a two-dimensional Ornstein-Uhlenbeck process, whose steady-state distribution takes the form [33, 65]

$$p_\infty(x, \eta) = \frac{e^{-\frac{1}{2}\mathbf{q}^\top \mathbf{C}^{-1} \mathbf{q}}}{\sqrt{(2\pi)^2 \det \mathbf{C}}}, \quad (8)$$

where

$$\mathbf{C} = \begin{pmatrix} \frac{\gamma}{k_2} [D + D_a \rho] & \sqrt{\frac{D_a}{2}} \rho \\ \sqrt{\frac{D_a}{2}} \rho & \frac{1}{2\tau_a} \end{pmatrix}, \quad \rho = \frac{1}{1 + \frac{k_2 \tau_a}{\gamma}}. \quad (9)$$

Taking (8) as the initial distribution, $p_0(x_0, \eta_0) = p_\infty(x_0, \eta_0)$, we can write the path weight (4) as (see also (5))

$$\begin{aligned} \mathbf{p}[\bar{x}] &\propto \int \mathcal{D}\bar{\eta} p_\infty(x_0, \eta_0) \exp \int_0^\tau \dagger \left\{ -\frac{1}{4D} \left[\dot{x}_t - v_t - \sqrt{2D_a} \eta_t \right]^2 \right. \\ &\quad \left. - \frac{\tau_a^2}{2} \left[\dot{\eta}_t + \frac{1}{\tau_a} \eta_t \right]^2 - \frac{1}{2} \frac{\partial v_t}{\partial x} \right\} \\ &= \int \mathcal{D}\bar{\eta} \exp \left\{ \int_0^\tau \dagger \left[-\frac{(\dot{x}_t - v_t)^2}{4D} - \frac{1}{2} \frac{\partial v_t}{\partial x} \right] - \frac{1}{2} \bar{C}_{11} x_0^2 \right. \\ &\quad \left. + \int_0^\tau \dagger \left[\frac{\sqrt{2D_a}}{2D} (\dot{x}_t - v_t) - \delta(t) \bar{C}_{12} x_t \right] \eta_t \right. \\ &\quad \left. - \frac{1}{2} \int_0^\tau \dagger \int_0^\tau \dagger' \eta_t V_{\text{HP}}(t, t') \eta_{t'} \right\} \end{aligned} \quad (10)$$

after partial integration of the $\dot{\eta}_t$ terms in the second equality, and with the abbreviation

$$\bar{\mathbf{C}} = \begin{pmatrix} \bar{C}_{11} & \bar{C}_{12} \\ \bar{C}_{12} & \bar{C}_{22} \end{pmatrix} = \mathbf{C}^{-1} = \frac{1}{D + D_a \rho^2} \begin{pmatrix} k_2/\gamma & -\sqrt{2D_a} \frac{k_2 \tau_a}{\gamma} \rho \\ -\sqrt{2D_a} \frac{k_2 \tau_a}{\gamma} \rho & 2\tau_a (D + D_a \rho) \end{pmatrix} \quad (11)$$

for the (symmetric) inverse of \mathbf{C} . The differential operator $V_{\text{HP}}(t, t')$ reads

$$V_{\text{HP}}(t, t') = \delta(t - t') \left[-\tau_a^2 \partial_{t'}^2 + 1 + \frac{D_a}{D} + \delta(t') (-\tau_a^2 \partial_{t'} - \tau_a + \bar{C}_{22}) + \delta(\tau - t') (\tau_a^2 \partial_{t'} + \tau_a) \right]. \quad (12)$$

Performing the Gaussian integral over $\bar{\eta}$ we obtain

$$\begin{aligned} \mathbf{p}[\bar{x}] \propto \exp \left\{ \int_0^\tau \dagger \int_0^\tau \dagger' \left[-\frac{1}{4D} \left(\dot{x}_t + \frac{k_2}{\gamma} x_t \right) \left[\delta(t-t') - \frac{D_a}{D} \Gamma_{\text{HP}}(t, t') \right] \left(\dot{x}_{t'} + \frac{k_2}{\gamma} x_{t'} \right) \right] \right. \\ \left. - \int_0^\tau \dagger \frac{\sqrt{2D_a}}{2D} \bar{C}_{12} \Gamma_{\text{HP}}(t, 0) \left(\dot{x}_t + \frac{k_2}{\gamma} x_t \right) x_0 \right. \\ \left. - \frac{1}{2} [\bar{C}_{11} - \bar{C}_{12}^2 \Gamma_{\text{HP}}(0, 0)] x_0^2 \right\}, \end{aligned} \quad (13)$$

where we have plugged in $v_t = -k_2 x_t / \gamma$. Moreover, $\Gamma_{\text{HP}}(t, t')$ denotes the operator inverse of $V_{\text{HP}}(t, t')$ in the sense that $\int_0^\tau \dagger' V_{\text{HP}}(t, t') \Gamma_{\text{HP}}(t', t'') = \delta(t - t'')$ (since the operator $V_{\text{HP}}(t, t')$ is diagonal in t and t' , the integral simplifies into a differential equation with $\Gamma_{\text{HP}}(t', t'')$ being its Green's function, see Appendix A). It can be constructed by a suitable extension of the procedure in [13] (see Appendix A),

$$\Gamma_{\text{HP}}(t, t') = \frac{\kappa_{+-} e^{-\lambda|t-t'|} + \kappa_{-+} e^{-\lambda(2\tau-|t-t'|)} - \kappa_{++} e^{-\lambda(t+t')} - \kappa_{--} e^{-\lambda(2\tau-t-t')}}{2\tau_a^2 \lambda (\kappa_{+-} - \kappa_{-+} e^{-2\lambda\tau})}. \quad (14)$$

with the abbreviations

$$\kappa_{\pm\pm} = \kappa_{\pm} (1 - \kappa_{\pm} \tau_a / \bar{C}_{22}) , \quad \kappa_{\pm} = 1 \pm \sqrt{1 + D_a / D}, \quad (15)$$

and $\lambda = \sqrt{1 + D_a / D} / \tau_a$. The first subscript in $\kappa_{\pm\pm}$ refers to the first κ_{\pm} on the right-hand side of its definition and the second subscript to the second κ_{\pm} .

Expression (13) together with the Green's function $\Gamma_{\text{HP}}(t, t')$ is thus the path probability density for a Brownian particle trapped in a harmonic potential and driven by an active Ornstein-Uhlenbeck process, when the two start out in a joint steady state. To compare to the case of independent initial conditions, which we have studied in [13] and which we briefly re-capitulate in Section 5 below, we observe that in this case $\bar{C}_{12} = 0$ and $\bar{C}_{22} = 2\tau_a$, so that we recover (21) as stated below when using $1 - \kappa_{\pm}/2 = \kappa_{\mp}/2$.

The path probability density for the *time-reversed* trajectories \tilde{x} is given by the same expression (13) (just equipping all x -symbols with a tilde), because there is no external driving protocol, and the system remains in its stationary state at all times along the forward trajectory so that the initial condition for the backward trajectory is again the steady-state distribution (8). Using $\tilde{x}(t) = x(\tau - t)$ and $\tilde{x}_0 = x(\tau) = x_{\tau}$, we can then express $\mathbf{p}[\tilde{x}]$ in terms of the forward path. The resulting expression looks similar to (13), but with opposite sign for all \dot{x}_t -terms, x_0 substituted by x_{τ} , and the replacements $t \rightarrow \tau - t$, $t' \rightarrow \tau - t'$ in all non-trivial time-arguments of Γ_{HP} .

With these results we can finally calculate $\Delta\Sigma[\bar{x}]$ as defined in (6),

$$\begin{aligned} \frac{\Delta\Sigma[\bar{x}]}{k_B} = & \frac{1}{D} \int_0^\tau \dagger \int_0^\tau \dagger' \left\{ \dot{x}_t \left(-\frac{k_2}{\gamma} x_{t'} \right) \left[\delta(t-t') - \frac{D_a}{D} \bar{\Gamma}_{\text{HP}}(t, t') \right] \right. \\ & + \frac{D_a}{4D} \dot{x}_t \dot{x}_{t'} \Delta\Gamma_{\text{HP}}(t, t') + \frac{D_a}{4D} \left(\frac{k_2}{\gamma} \right)^2 x_t x_{t'} \Delta\Gamma_{\text{HP}}(t, t') \left. \right\} \\ & - \frac{\sqrt{2D_a}}{2D} \int_0^\tau \dagger \left\{ \dot{x}_t \bar{C}_{12} \left[\Gamma_{\text{HP}}(t, 0) x_0 + \Gamma_{\text{HP}}(\tau - t, 0) x_\tau \right] \right. \\ & + \frac{k_2}{\gamma} x_t \bar{C}_{12} \left[\Gamma_{\text{HP}}(t, 0) x_0 - \Gamma_{\text{HP}}(\tau - t, 0) x_\tau \right] \left. \right\} \\ & + \frac{1}{2} [\bar{C}_{11} - \bar{C}_{12}^2 \Gamma_{\text{HP}}(0, 0)] (x_\tau^2 - x_0^2) . \end{aligned} \quad (16)$$

To arrive at this expression we have used the symmetry $\Gamma_{\text{HP}}(t, t') = \Gamma_{\text{HP}}(t', t)$, and we have introduced the abbreviations $\bar{\Gamma}_{\text{HP}} = \frac{1}{2} [\Gamma_{\text{HP}}(t, t') + \Gamma_{\text{HP}}(\tau - t, \tau - t')]$ and $\Delta\Gamma_{\text{HP}} = \Gamma_{\text{HP}}(t, t') - \Gamma_{\text{HP}}(\tau - t, \tau - t')$ for the mean and the difference of $\Gamma_{\text{HP}}(t, t')$ and its time-reversed counterpart $\Gamma_{\text{HP}}(\tau - t, \tau - t')$.

4.2. Path-wise reversibility

Substituting the inverse (11) of (9) into (16), we can show that $\Delta\Sigma[\bar{x}] = 0$, and thus, according to (6),

$$\frac{\mathfrak{p}[\bar{\tilde{x}}]}{\mathfrak{p}[\bar{x}]} = 1 \quad (17)$$

exactly, for any values of the system parameters. This reversibility holds on the level of individual steady-state trajectories of arbitrary duration τ . Transients (towards the steady state) may still be irreversible, but are not captured in (17) by construction, since we are interested in characterizing the (ir)reversibility of the steady state of a trapped AOUP and therefore calculated $\Gamma_{\text{HP}}(t, t')$ for an initial setup corresponding to the joint steady state of the Brownian particle and the active Ornstein-Uhlenbeck fluctuations.

The details of the derivation of (17) involve some rather tedious manipulations of the log ratio (16) and are thus relegated to Appendix B. The crucial insight behind these calculations is to integrate by parts in order to move all time derivatives from the particle trajectory to the memory kernel $\Gamma_{\text{HP}}(t, t')$, generating additional terms with one or two time points on the boundary $t = 0$ or $t = \tau$. Then we can demonstrate that all three types of contributions to (16), namely the two-time integrals over t and t' , the one-time integrals with the other time point lying on the boundary, and the boundary contributions (which include the integral involving $\delta(t - t')$), vanish individually.

The ratio (17) tells us that for the steady state in a harmonic trap we will observe every individual trajectory with a probability which is exactly equal to the probability for observing the same trajectory in reversed time, i.e. probabilities to observe forward and backward paths coincide and the process appears reversible. In a corresponding experiment in which only the position of the particle is measured, it is therefore

impossible to determine an “arrow of time”. Given a movie of the particle dynamics, we will be unable to tell whether it is being played forwards or backwards, no matter how long it is, i.e. no matter how many data points we have. As argued above, the unbiased, time-correlated fluctuations do not favor a particular direction in space or time, so we may have expected this result. In the following Sections we will check if this reversibility property is specific to the combination of an Ornstein-Uhlenbeck noise modeling the active forces with a harmonic trapping potential, or if it is valid for more general confining potentials.

Before doing so, we remark that the situation is different in a scenario in which the active fluctuations are an observable degree of freedom. If we were somehow able to measure the force $\sqrt{2D_a}\eta(t)$ stemming from the active fluctuations, we could compare probabilities for forward and backward histories of the *joint process* $(x(t), \eta(t))$. In this x - η phase space, there is always an effective “torque” (a nonconservative force component) as can be seen from the fact that $\eta(t)$ drives $\dot{x}(t)$, but there is no feedback from $x(t)$ to $\dot{\eta}(t)$ (see Eqs. (1) and (2)). Hence, there is a “current” in the $(x(t), \eta(t))$ dynamics in the form of a net average rotation, breaking the phase space symmetry, which will allow to distinguish forward from backward processes on statistical grounds (see, e.g., Ref. [66] and Fig. 1 therein). For the particle coordinates alone, a similar situation can arise in more than one spatial dimension under the influence of a mechanical torque [67–73].

4.3. Remark on $d > 1$ dimensions

It is straightforward to convince ourselves that the same path-wise reversibility holds for the steady state of an AOUP trapped in a harmonic potential of higher than one dimension (or many non-interacting AOUPs in such a potential). In that case, the equations of motion read

$$\dot{\mathbf{x}}(t) = -\mathbf{K}\mathbf{x}(t) + \sqrt{2D_a}\boldsymbol{\eta}(t) + \sqrt{2D}\boldsymbol{\xi}(t), \quad (18a)$$

$$\dot{\boldsymbol{\eta}}(t) = -\frac{1}{\tau_a}\boldsymbol{\eta}(t) + \frac{1}{\tau_a}\boldsymbol{\zeta}(t), \quad (18b)$$

with vector quantities of dimension $d > 1$ as obvious generalizations of the scalar quantities from (1) and (2), and a positive definite symmetric $d \times d$ tensor \mathbf{K} specifying the harmonic trap. Note that the different dimensions (or particles) have identical properties concerning thermal and active fluctuations, i.e. the $d \times d$ tensors in front of $\boldsymbol{\xi}(t)$ and $\boldsymbol{\eta}(t)$ in (18a) and $\boldsymbol{\zeta}(t)$ in (18b) are all proportional to the identity tensor.

Since \mathbf{K} is symmetric we can diagonalize it with an orthogonal $d \times d$ tensor \mathbf{O} . The rotated thermal and active noise processes $\mathbf{O}\boldsymbol{\xi}(t)$ and $\mathbf{O}\boldsymbol{\eta}(t)$ have the same statistical properties as the original ones. In particular, their components are mutually independent, such that the set of $2d$ equations (18a) and (18b) decouples into d independent pairs of equations of the form (1), (2).

As a consequence, we can write the path probability density $\mathbf{p}[\bar{\mathbf{x}}]$ for the d -dimensional particle trajectories $\bar{\mathbf{x}}$ as a product of d independent path probability

densities for the individual components. Accordingly, the irreversibility measure $\Delta\Sigma[\bar{x}]$ is a sum of d independent contributions of the form (16), which all vanish identically.

5. Double-well potential

In this Section, we consider the AOUP dynamics (1) in a double-well potential like the one shown in Fig. 1, corresponding to choosing $k_4 > 0$ and $k_2 < 0$ in (7). Unlike the purely harmonic trap from the previous Section, this case does not allow for calculating $\Delta\Sigma[\bar{x}]$ with the joint steady state as initial distribution, because the analytical form of this joint steady state is unknown. We therefore use the results from [13], which we have obtained under the assumption that the active fluctuations alone are in their steady state, independent of the initial position x_0 , i.e.

$$p_0(x_0, \eta_0) = p_0(x_0)p_0(\eta_0|x_0) = p_0(x_0)p_0(\eta_0) = p_0(x_0) \sqrt{\frac{\tau_a}{\pi}} e^{-\tau_a \eta_0^2}, \quad (19)$$

where $\sqrt{\frac{\tau_a}{\pi}} e^{-\tau_a \eta^2}$ is the steady state distribution of the process (2). For reasonable x_0 , we are thus a short transient away from the joint steady state, with negligible effects on the long-term steady state dynamics of the system.

The log ratio of path probabilities from [13] for a fixed initial position x_0 of the active particle reads

$$\begin{aligned} \frac{\Delta\Sigma[\bar{x}]}{k_B} &= \ln \frac{\mathbf{p}[\bar{x}]}{\mathbf{p}[\tilde{x}]} = \ln \frac{\mathbf{p}[x|x_0]}{\mathbf{p}[\tilde{x}|\tilde{x}_0]} + \ln \frac{p(x_0)}{p(\tilde{x}_0)} \\ &= \frac{1}{D} \int_0^\tau \int_0^\tau \dot{x}_t v_{t'} \left[\delta(t-t') - \frac{D_a}{D} \Gamma(t, t') \right] + \ln \frac{p(x_0)}{p(x_\tau)}, \end{aligned} \quad (20)$$

where $v_t = -U'(x(t))/\gamma$ and

$$\Gamma(t, t') = \left(\frac{1}{2\tau_a^2 \lambda} \right) \frac{\kappa_+^2 e^{-\lambda|t-t'|} + \kappa_-^2 e^{-\lambda(2\tau-|t-t'|)} - \kappa_+ \kappa_- [e^{-\lambda(t+t')} + e^{-\lambda(2\tau-t-t')}]}{\kappa_+^2 - \kappa_-^2 e^{-2\lambda\tau}}, \quad (21)$$

with $\lambda = \sqrt{1 + D_a/D}/\tau_a$ and $\kappa_\pm = 1 \pm \sqrt{1 + D_a/D}$, as before. The first term in (20) has two contributions in the double integral, one involving the non-local kernel $\Gamma(t, t')$, which vanishes for $D_a = 0$ and is therefore named the “colored-noise contribution”,

$$\frac{\Delta\Sigma_c[\bar{x}]}{k_B} = -\frac{D_a}{D^2} \int_0^\tau \int_0^\tau \dot{x}_t v_{t'} \Gamma(t, t'); \quad (22a)$$

and a term proportional to $\delta(t-t')$, which survives even for $D_a = 0$ and is thus called “white-noise contribution”,

$$\frac{\Delta\Sigma_w[\bar{x}]}{k_B} = \frac{1}{D} \int_0^\tau \dot{x}_t v_t = \frac{1}{k_B T} [U(x_0) - U(x_\tau)]. \quad (22b)$$

The second term in (20) quantifies the irreversibility associated with the boundary distributions at initial and final points in time, and is usually interpreted as the change in system entropy between the initial and final configurations [13]. It is non-extensive in the length τ of the trajectory and thus turns out to be negligible for sufficiently long trajectories compared to the time-extensive contributions in $\Delta\Sigma[\bar{x}]$.

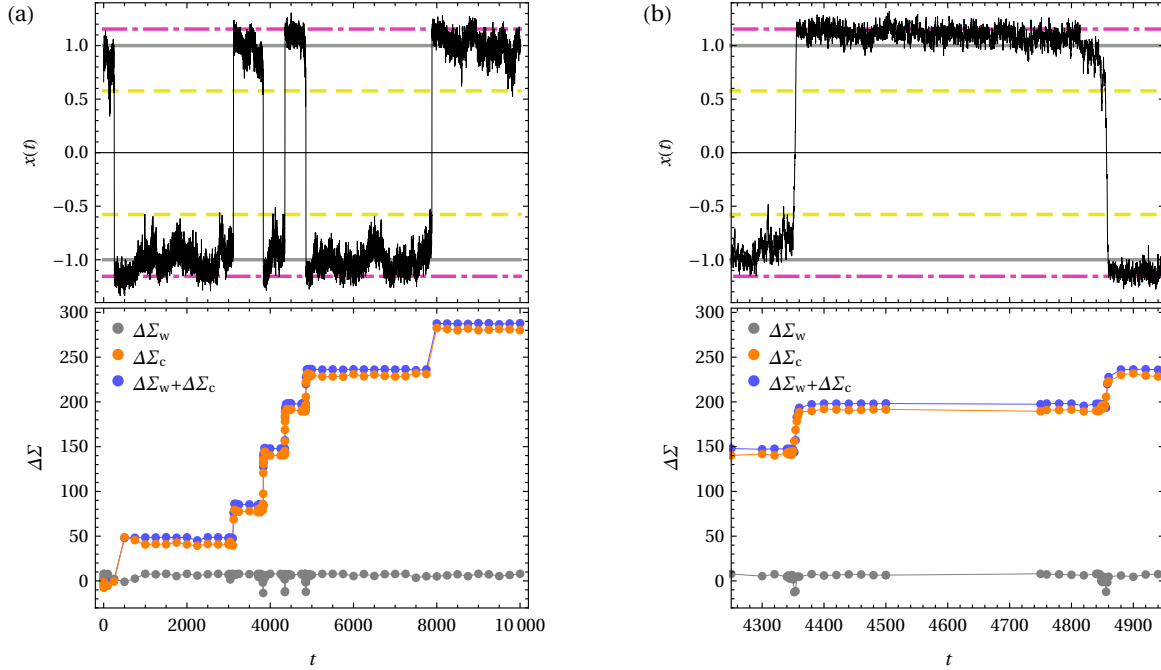


Figure 2. (a) A single trajectory (top) and corresponding irreversibility productions $\Delta\Sigma$ (bottom). (b) Close-up of the same trajectory (top) and irreversibility productions (bottom) for the time interval from about 4300 to 4900. In the lower panels, the dots mark the time points for which the values of $\Delta\Sigma_w$ (grey dots) and $\Delta\Sigma_c$ (orange dots) have been evaluated from the integrals in (22b) and (22a); the connecting lines serve as a guide to the eye. For numerical reasons and since the integrals in (22a) have a smoothing effect anyway, we chose a time-resolution considerably coarser than the original trajectory. Yellow dashed and purple dash-dotted lines in the top panels represent the specific positions in the potential as marked in Fig. 1, solid gray lines illustrate the positions of the potential minima. Unlike for a passive particle, for an AOUP the maxima of the steady-state distribution do not coincide with the potential minima due the active driving. Parameter values: $k_4 = 1$, $k_2 = -1$, $\tau_a = 250$, $D_a = 10$, $D = 0.01$, $\gamma = 1$, $k_B = 1$.

5.1. First numerical experiments

A typical trajectory is plotted in the upper panel of Fig. 2(a). The irreversibility $\Delta\Sigma$ as a function of the trajectory duration is shown in the lower panels (blue), along with a splitting into white-noise contributions $\Delta\Sigma_w$ (gray) and colored-noise contributions $\Delta\Sigma_c$ (orange); the boundary term $\ln \frac{p(x_0)}{p(\bar{x}_0)}$ would typically be of the order of $\Delta\Sigma_w$ and has been neglected in the plots. As it should, the white-noise contribution becomes stationary pretty soon and does not grow extensively since the corresponding stochastic integral depends only on the initial and final points of the trajectory. The active contribution, however, increases sharply whenever the particle jumps from one minimum to the other. Hence, we find that the steady-state trajectories in a quartic potential are irreversible, and that the jumps between the two potential minima render the dynamics irreversible, even though there is no net current from one side to the other. This means that it is in principle possible to tell apart trajectories which run forward in time from those which

run backward in time.

5.2. Explaining irreversibility

The quartic potential for $k_4 > 0$, $k_2 < 0$ and the resulting force are sketched in Fig. 1. The potential has a local maximum at $x_{\max} = 0$ and two minima at $x_{\min}^{\pm} = \pm\sqrt{-k_2/k_4}$ (solid gray lines in Fig. 1). There are also two inflection points at $x_{\text{inf}}^{\pm} = \pm\sqrt{-k_2/3k_4} = x_{\min}/\sqrt{3}$, where the force's magnitude reaches a local extremum (dashed yellow lines in Fig. 1). For every inflection point, there is one point on the opposite side of the origin where the force takes the same value as it does at x_{inf}^{\pm} (dash-dotted purple lines in Fig. 1). We denote these conjugate equal-force points by $x_{\text{jmp}}^{\pm} = \mp\sqrt{-4k_2/3k_4} = 2x_{\text{inf}}^{\mp}$, such that $U'(x_{\text{jmp}}^{\pm}) = U'(x_{\text{inf}}^{\pm})$.

Fily [74] analyzed such a setup in the limit of high persistence, for which τ_a is by far the largest time scale in the system (see also [56, 75] for related studies). He showed that, asymptotically for $\tau_a \rightarrow \infty$, the particle is never found in the region $(x_{\text{inf}}^-, x_{\text{inf}}^+)$ between the inflection points. To explain this observation, assume that the potential barrier around the origin is sufficiently high so that purely thermally induced crossings of the barrier are rare. However, if the active forcing is large enough to counter the restoring potential forces when moving uphill towards the barrier, the particle can climb up the hill towards the origin and reach the inflection point of maximum counterforce. Due to persistence of the active fluctuations, the particle will then continue to push in the direction of its active drive, and speed up because the opposing force will be weaker until the origin is reached, from where on active and potential forces will even point in the same direction. The active forces will only be balanced again once the particle approaches the conjugate equal-force point beyond the barrier, where it will thus be slowed down and “stopped” eventually. The transition from one side of the double-well potential to the other thus looks like a “sudden jump”, in particular on the time-scale τ_a of the active fluctuations. When the active fluctuations change sign, the same process can then occur in the opposite direction.

As a consequence, the trajectories of such an active particle show hysteresis-like behavior and exhibit a clear signature of an “arrow of time” despite the conservative, time-independent confining forces: The particle preferentially “jumps” from an inflection point x_{inf}^{\pm} (dashed yellow lines in Fig. 1) to the corresponding equal-force point x_{jmp}^{\pm} on the other side of the barrier (dash-dotted purple lines in Fig. 1), but (practically) never the other way (from x_{jmp}^{\pm} to x_{inf}^{\pm}). We can nicely see this behavior in Fig. 2(b), showing close-up views of two transitions from the trajectory plotted in Fig. 2(a). If we were to see a trajectory dominated by “jumps” from the points x_{jmp}^{\pm} to the points x_{inf}^{\pm} , we are most likely watching a trajectory which is “played” backward in time. This intuitive picture suggests that the irreversibility of trajectories is encoded predominantly in the “jumps” between the potential wells. Figure 2 highlights that our dynamical measure $\Delta\Sigma[\bar{x}]$, eq. (20), identifies these “jumps” as the principle source of irreversibility, too.

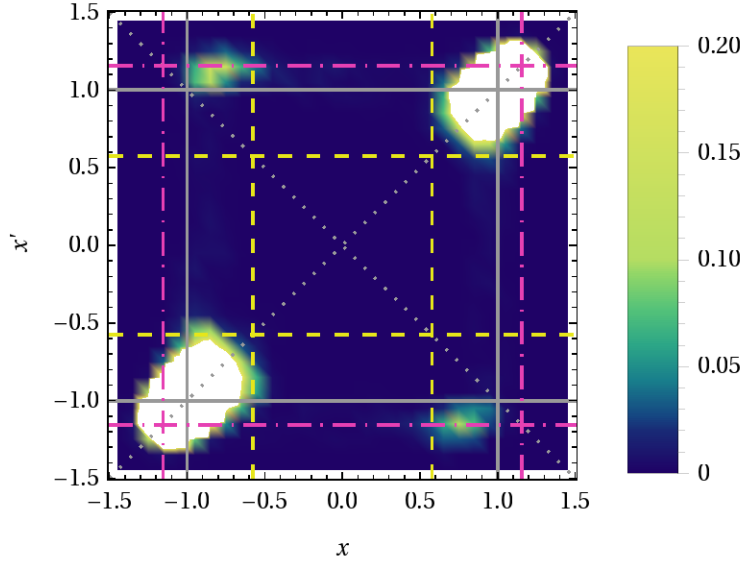


Figure 3. Two-point probability density $p(x', t'; x, t)$ for step size $t' - t = 25$. Potential minima are marked by solid gray lines. Inflection points x_{inf}^{\pm} are marked by dashed yellow lines. The corresponding jump target points x_{jmp}^{\pm} are marked by dash-dotted purple lines, see also Fig. 1. The dotted gray lines mark the diagonals $x = x'$ and $x = -x'$ and guide the eye to assess the (a)symmetry of the plot. Parameter values as in Fig. 2.

The irreversibility of trajectories also becomes apparent by inspection of the two-point probability density $p(x', t'; x, t)$, shown for the time delay $t' - t = 25$ in Fig. 3. It illustrates the probability of observing the particle at a certain position x in the potential at time t and at position x' at a later time $t' = t + 25$. The mirror symmetry $x \leftrightarrow -x$ of the potential is reflected by the point symmetry in Fig. 3 with respect to the origin $(0, 0)$. The potential minima are located at the solid gray lines. The bright spots around the crossings of these lines on the diagonal $x = x'$ (lower left and upper right corner in Fig. 3) correspond to a high probability density and indicate that the particle is most likely to stay in the potential well it is starting from at the beginning of the time-interval $t' - t = 25$. The other two bright spots in Fig. 3 (upper left corner and lower right corner) represent the “jumps” from one side of the potential to the other side. Their irreversibility is visible in the asymmetry of the probability density spots with respect to the diagonal $x = x'$. The starting positions (x coordinates) at time t are close to the inflection points $x \approx x_{\text{inf}}^{\pm}$ (vertical dashed yellow lines), while the final positions (x' coordinates) are the jump-target points $x' \approx x_{\text{jmp}}^{\pm}$ (horizontal dash-dotted purple lines). Analogous density spots that would correspond to the opposite “jumps” from $x \approx x_{\text{jmp}}^{\pm}$ to $x' \approx x_{\text{inf}}^{\pm}$ are absent, implying that any steady-state trajectory of the AOUP trapped in a double-well potential becomes more and more irreversible over time. In this sense it “produces irreversibility” and encodes an “arrow of time”.

5.3. Exploring irreversibility

As pointed out above, the clear hysteresis-like behavior and its irreversibility are associated with the high persistence of the active fluctuations induced by large τ_a . We expect, however, that particle trajectories become fully reversible in the strict limit $\tau_a \rightarrow \infty$, in which the dynamics of $\eta(t)$ is “frozen” and the active velocity $\sqrt{2D_a}\eta(t) = \sqrt{2D_a}\eta(0)$ remains constant for all times. In that case the constant active velocity $\sqrt{2D_a}\eta(0)$ can be absorbed into the potential as a tilting force, $U(x) - \gamma\sqrt{2D_a}\eta(0)x$, such that (1) effectively turns into a Langevin-equation for a *passive* Brownian particle confined in a tilted double-well potential. The steady state is then identical to thermal equilibrium in the tilted potential, and therefore any particle trajectory is reversible (on the time-scales that are shorter than τ_a).

For smaller τ_a -values, on the other hand, we may expect that a “weakened” or “smoothed-out” form of the hysteresis-like behavior is still producing irreversibility, even if the irreversibility of the trajectories might not be visible to the naked eye any more in the lucidity it is displayed in Fig. 2. To study the effect of decreasing τ_a , there are two possible scenarios: On the one hand, we can keep the active diffusion D_a fixed, such that the process $\sqrt{2D_a}\eta(t)$ approaches a thermal white-noise process with diffusion D_a as $\tau_a \rightarrow 0$. Then, the particle feels an effective total temperature of $\gamma(D + D_a)/k_B = T + \gamma D_a/k_B$. Alternatively, we can require that the active velocity $v_a = \sqrt{D_a/\tau_a}$ remains fixed (which may be the more natural limit when taking the AOUP as an approximation for an active Brownian particle [28, 38, 39]). Then, the overall intensity decreases as τ_a becomes smaller until the particle just feels the thermal fluctuations at temperature $\gamma D/k_B = T$ as $\tau_a \rightarrow 0$. In both cases, the limit $\tau_a \rightarrow 0$ turns (1) into an equation of motion for a *passive* Brownian particle, so that again all trajectories become reversible. In the following, we will explore the regime of intermediate τ_a -values for both of the scenarios mentioned above, namely constant active diffusion and constant active velocity. For a discussion of the $\tau_a \rightarrow 0$ and $\tau_a \rightarrow \infty$ limits for an AOUP in a slightly different setting we refer to Ref. [66].

5.3.1. Decreasing active correlation time at constant active diffusion. We first consider decreasing τ_a for fixed $D_a = 10$. Fig. 4 shows trajectories for $\tau_a = 50$ (right), $\tau_a = 1$ (middle) and $\tau_a = 0.1$ (left) along with their irreversibility productions. The production rate $\Delta\Sigma/\tau$ is larger for $\tau_a = 50$ than it is for $\tau_a = 250$ in Fig. 2, and grows even further as $\tau_a = 1$. At the same time the frequency of jumps increases as τ_a is lowered. However, eventually the production rate decreases again ($\tau_a = 0.1$) and is expected to reach zero in the white-noise limit $\tau_a \rightarrow 0$, while the number of “jumps” continues to grow. In this limit, diffusion is so strong that the potential barrier around the origin affects the dynamics only marginally. We remark that while $\Delta\Sigma$ is apparently negative in the passive white-noise limit, the full entropy production is only obtained upon adding the system contributions (the second term in (20)) and must be zero in the steady state since for passive Brownian motion the steady state corresponds to thermal equilibrium.

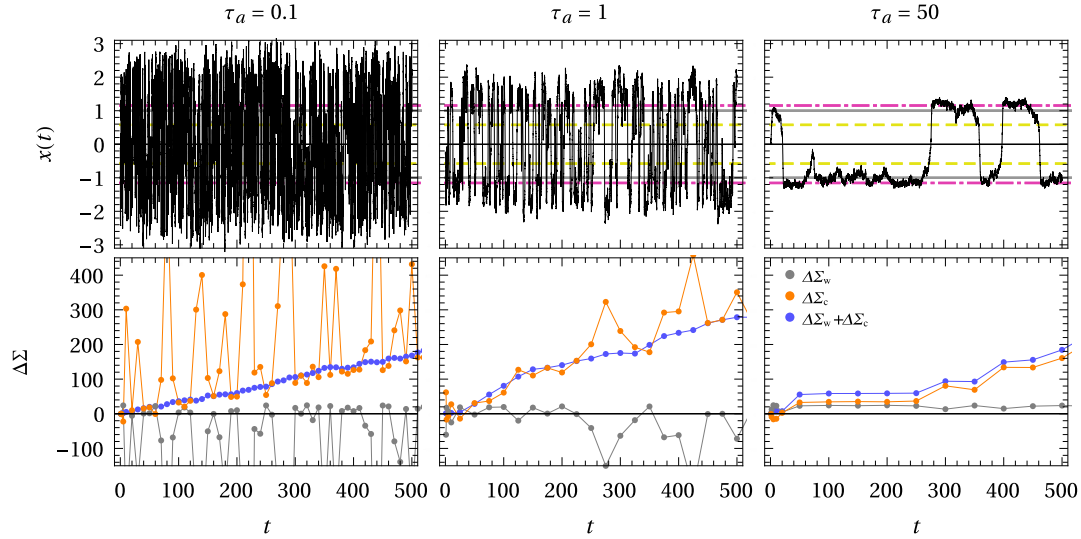


Figure 4. Single trajectories (top) and corresponding irreversibility productions $\Delta\Sigma$ (bottom) for three systems with different active correlation times smaller than $\tau_a = 250$ from Fig. 2: $\tau_a = 0.1$ (left), $\tau_a = 1$ (middle), and $\tau_a = 50$ (right). All other parameter values are as in Fig. 2. The frequency of jumps increases as τ_a decreases and the self-propulsion force switches direction more often. In the lower panels, the dots mark the time points for which the values of $\Delta\Sigma_w$ (grey dots) and $\Delta\Sigma_c$ (orange dots) have been evaluated from the integrals in (22b) and (22a); the connecting lines serve as a guide to the eye. The time-resolution is considerably lower than for the trajectories in the upper panels. In particular for smaller values of τ_a the increasing number of jumps in the trajectory is not resolved but rather smoothened-out in the $\Delta\Sigma$ curves. The horizontal yellow dashed and purple dash-dotted lines in the top panels represent the specific positions in the potential as marked in Fig. 1, solid gray lines illustrate the positions of the potential minima.

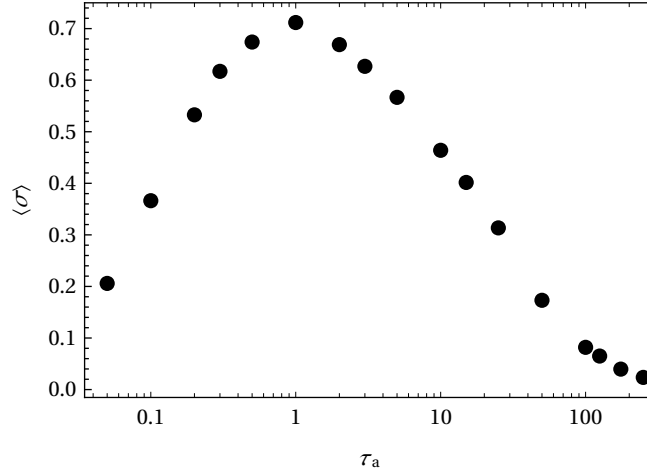


Figure 5. Irreversibility production rate $\langle\sigma\rangle$ in the quartic double-well potential as a function of the active correlation time τ_a for fixed active diffusion $D_a = 10$. All other parameter values are as in Fig. 2.

In our case, however, the total entropy production would assume a small positive value from a short transient phase, because we are not starting from the (joint) steady state and thus are slightly out of equilibrium in the beginning.

The dependence of the average irreversibility production rate

$$\langle\sigma\rangle = \lim_{\tau \rightarrow \infty} \langle\Delta\Sigma(\tau)\rangle/\tau \quad (23)$$

on the active correlation time is summarized in Fig. 5. We can see the tendency towards vanishing irreversibility production rate in the two limits $\tau_a \rightarrow \infty$ and $\tau_a \rightarrow 0$ as discussed above, and a maximum of irreversibility production at around $\tau_a \approx 1$. Surprisingly, the irreversibility production rate at the persistence time $\tau_a = 250$, for which we can observe the distinct hysteresis-like behavior and discern an “arrow of time” in the particle trajectories by naked eye (cf. Figs. 2 and 3), is about a factor 20 smaller than the maximal rate at $\tau_a \approx 1$. We might expect that this is due to a maximized rate of “jumps” between potential wells at $\tau_a \approx 1$, maximizing the number of irreversible hysteresis-like cycles. Intuitively, a maximal “jump” rate might occur when the persistence time τ_a of the active fluctuations is of the order of the typical duration of a “jump” from one potential well to the other, because then the next “jump” is initiated right after having finished the previous one.

5.3.2. Decreasing active correlation time at constant active velocity. The second option when taking the limit $\tau_a \rightarrow 0$ is to keep the self-propulsion velocity $v_a = \sqrt{D_a/\tau_a}$ of the particle fixed. In the high-persistence case from Fig. 2 above, its value is $v_a = 1/5$. Data for three correlation times smaller than $\tau_a = 250$ are shown in Fig. 6. We observe that, compared to $\tau_a = 250$ in Fig. 2, the frequency of jumps first increases ($\tau_a = 100$ and $\tau_a = 10$) (note that the trajectories in Fig. 6 are about a factor 5 shorter than in Fig. 2), accompanied by an increase of irreversibility production. Eventually, however, the jump frequency decreases again ($\tau_a = 1$) until jumps become very rare. Summarizing, Fig. 7 shows the average irreversibility production rate $\langle\sigma\rangle$ from (23) as a function of τ_a (analogous to Fig. 5). Again, we can see the irreversibility production rate approaching zero in the limits $\tau_a \rightarrow \infty$ and $\tau_a \rightarrow 0$. The maximal rate is reached at around $\tau_a \approx 10 \dots 30$, and is roughly three times as large as the rate at $\tau_a = 250$, for which we have discussed the hysteresis-like behavior of the particle trajectories and the associated irreversibility in Sections 5.1 and 5.2 above. Compared to the finding in Fig. 5 for the constant- D_a scenario, the maximal irreversibility production rate in Fig. 7 occurs at about a 10 times larger value for τ_a . This observation is consistent with our intuitive explanation of matching time-scales τ_a and typical “jump times”, because the latter is dominated by the active self-propulsion velocity v_a , which has the value $v_a = \sqrt{10}$ at $\tau_a = 1$ in Fig. 5 and $v_a = 1/5$ in Fig. 7, with roughly a factor 10 difference.

Finally, we would like to direct the reader’s attention to the left panel of Fig. 6. The particle is staying in one and the same potential well during the whole duration of the trajectory, i.e. it is not jumping between potential wells, but $\Delta\Sigma$ increases nevertheless (though at a much slower rate than during the jumps). It therefore seems that the

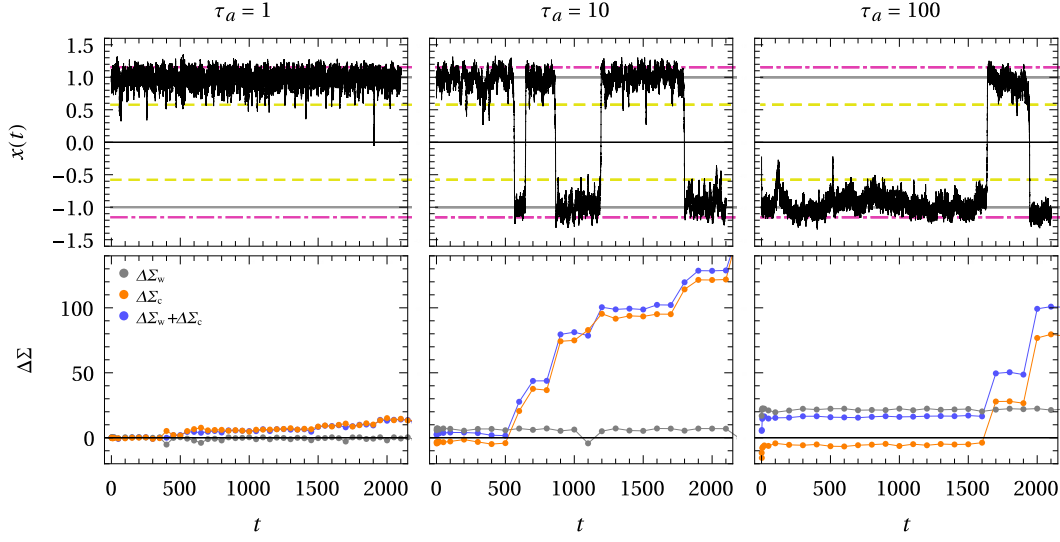


Figure 6. Single trajectories (top) and corresponding irreversibility productions $\Delta\Sigma$ (bottom) for three systems with different active correlation times smaller than $\tau_a = 250$ from Fig. 2: $\tau_a = 1$ (left), $\tau_a = 10$ (middle), and $\tau_a = 100$ (right). Here, the active velocity $v_a = \sqrt{D_a/\tau_a} = 1/5$ is kept constant, so that $D_a = 0.04$ (left), $D_a = 0.4$ (middle) and $D_a = 4.0$ (right), respectively. All other parameter values are as in Fig. 2. In the lower panels, the dots mark the time points for which the values of $\Delta\Sigma_w$ (grey dots) and $\Delta\Sigma_c$ (orange dots) have been evaluated from the integrals in (22b) and (22a); the connecting lines serve as a guide to the eye. The time-resolution is considerably lower than for the trajectories in the upper panels. The horizontal yellow dashed and purple dash-dotted lines in the top panels represent the specific positions in the potential as marked in Fig. 1, solid gray lines illustrate the positions of the potential minima.

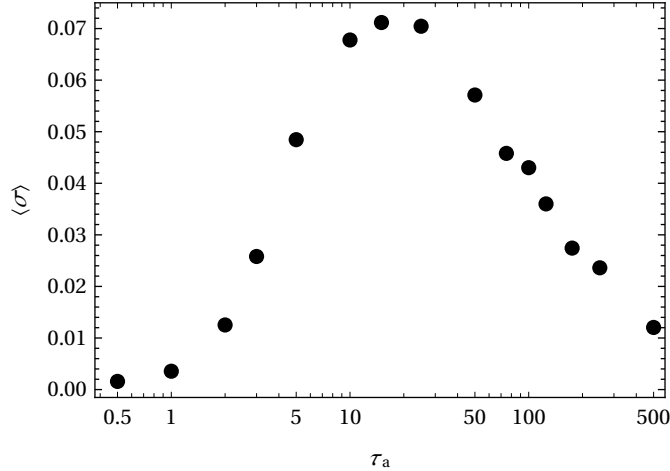


Figure 7. Irreversibility production rate $\langle\sigma\rangle$ in the quartic double-well potential as a function of the active correlation time τ_a for fixed active speed $v_a = 1/5$. All other parameter values are as in Fig. 2.

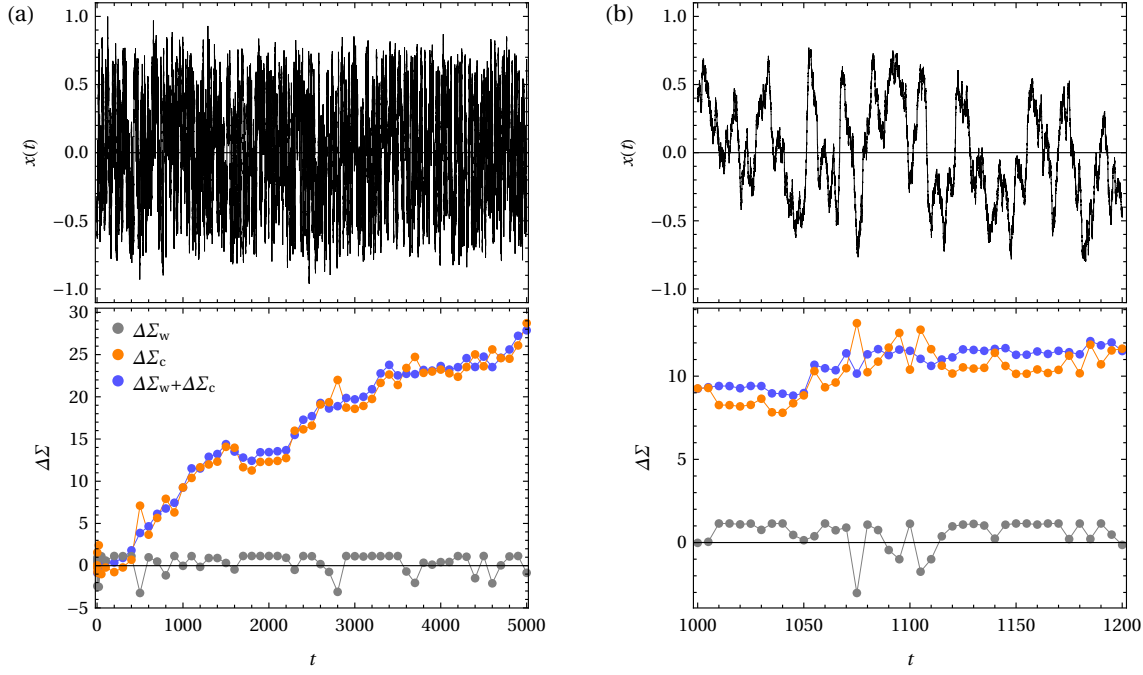


Figure 8. (a) A single trajectory (top) and corresponding irreversibility productions $\Delta\Sigma$ (bottom) in a quartic single-well potential ($k_4 = 1$, $k_2 = 0$) for the same dynamical parameters as in Fig. 6 (left panels) (i.e. $\tau_a = 1$, $D_a = 0.04$, $D = 0.01$, $\gamma = 1$, $k_B = 1$). (b) Close-up of the same trajectory (top) and irreversibility productions (bottom) for the time interval from about 1000 to 1200. In the lower panels, the dots mark the time points for which the values of $\Delta\Sigma_w$ and $\Delta\Sigma_c$ have been evaluated from the integrals in (22b) and (22a); the connecting lines serve as a guide to the eye.

steady state of an AOUP is irreversible even in a single-well potential, provided the potential is anharmonic (cf. Section 4). In the following Section, we are going to briefly investigate the irreversibility properties of an AOUP trapped in a quartic single-well potential.

6. Quartic single-well potential

In this Section, we turn to the case of the AOUP (1) moving in a quartic single-well potential with $k_4 > 0$ and $k_2 = 0$ in (7). Figure 8 shows a stationary-state trajectory (upper panels) of the AOUP together with the irreversibility production (lower panels) for the same parameters of the active fluctuations as in the leftmost panels of Fig. 6. Figure 10(a) displays the corresponding steady-state distribution. The effect of the active fluctuations is visible in the broadening of the distribution (compared to the Boltzmann distribution it would assume without activity), as the active fluctuations push the particle more towards the flanks of the potential. From Fig. 8(a), we see that the main contribution to irreversibility is due to the colored-noise memory kernel (22a) characteristic for the active fluctuations, while the thermal white-noise component does not produce irreversibility. Moreover, irreversibility seems to be produced more or less

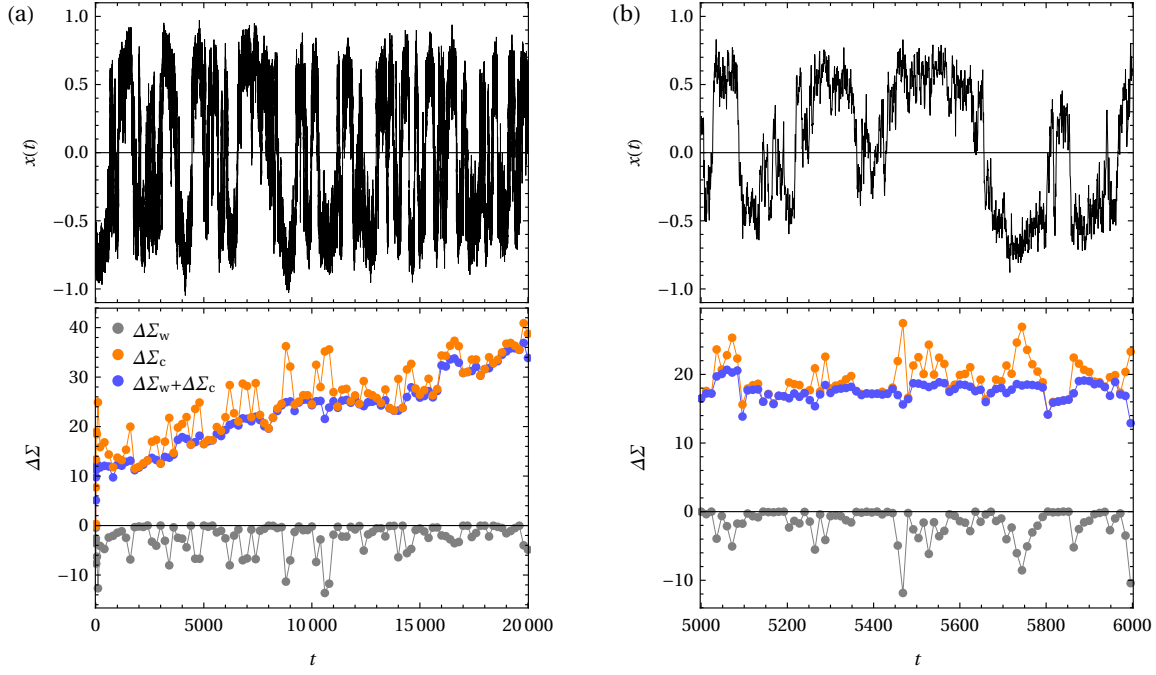


Figure 9. (a) A single trajectory (top) and corresponding irreversibility productions $\Delta\Sigma$ (bottom) in a quartic single-well potential ($k_4 = 1$, $k_2 = 0$) for the same dynamical parameters as in Fig. 2 (i.e. $\tau_a = 250$, $D_a = 10$, $D = 0.01$, $\gamma = 1$, $k_B = 1$). (b) Close-up of the same trajectory (top) and irreversibility productions (bottom) for the time interval from about 5000 to 6000. In the lower panels, the dots mark the time points for which the values of $\Delta\Sigma_w$ (grey dots) and $\Delta\Sigma_c$ (orange dots) have been evaluated from the integrals in (22b) and (22a); the connecting lines serve as a guide to the eye.

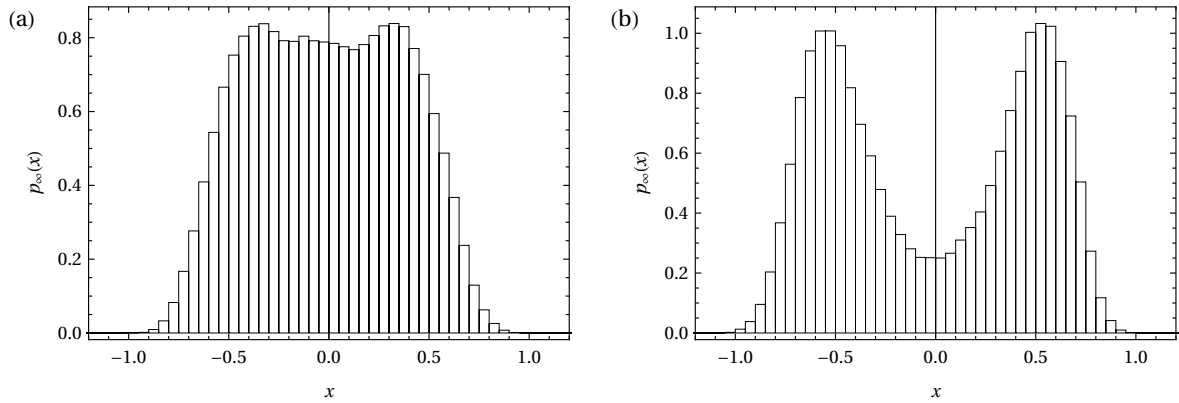


Figure 10. Numerically computed steady-state distributions $p_\infty(x)$ of the AOUP trapped in a quartic single-well potential ($k_4 = 1$, $k_2 = 0$ in (7)). (a) Parameter values as in Fig. 8 (i.e. $\tau_a = 1$, $D_a = 0.04$, $D = 0.01$, $\gamma = 1$, $k_B = 1$). (b) Parameter values as in Fig. 9 (i.e. $\tau_a = 250$, $D_a = 10$, $D = 0.01$, $\gamma = 1$, $k_B = 1$). Deviations from perfect mirror symmetry are due to statistical fluctuations.

continuously without being connected to specific features of the trajectory (like the “jumps” in the case of a double-well potential). This observation is confirmed by the closeup in Fig. 8(b), where it becomes apparent that the transition-like movement of the particle from one side of the potential well to the other is not accompanied by a distinct production of irreversibility. We can “enhance” these transitions by increasing the persistence time of the active fluctuations, such that the active forcing $\eta(t)$ pushes the particle to one side of the potential well for an extended period of time until $\eta(t)$ changes sign and drives the particle over to the other side. We show a corresponding trajectory (upper panels) and the associated irreversibility (lower panels) for $\tau_a = 250$ in Fig. 9 (and with $D_a = 10$, i.e. the same active fluctuations for which we could observe the “arrow of time” in the double-well potential, see Fig. 2). The trajectory now shows “jump-like” transitions between the two edges of the potential well at around ± 0.5 ; see, in particular, the closeup in Fig. 9(b), and the associated steady-state distribution in Fig. 10(b) with two peaks at the edges of the potential and a depleted zone in the middle. However, there is no clear indication that these “jump-like” transitions play a similar role as a source of irreversibility like in the double-well potential. In fact, the trajectory does not reveal any obvious features which would tell us that it is considerably less likely to observe the same trajectory in the stationary state but traced out backward in time.

From numerical simulations we find the maximal rate of irreversibility production in the quartic single-well potential ($k_4 = 1$, $k_2 = 0$) when varying τ_a according to the constant $v_a = \sqrt{D_a/\tau_a}$ scenario to be roughly 0.02 at around $\tau_a = 5$. Surprisingly, this maximal irreversibility production rate is only about a factor 3 smaller than the one in the double-well potential (see Fig. 7), even though in these two systems irreversibility is produced by significantly different physical processes on distinct scales (exploring the single quartic well vs. jumping between potential wells). Despite these contrasts, the similar irreversibility productions in the quartic single- and double-well potential imply that the likelihood of observing time-reversed trajectories on average decreases at comparable rates, and likewise the uncertainty when estimating the direction of the arrow of time based on $\langle \sigma \rangle$ [64].

7. Conclusions

Active matter systems are inherently driven out of equilibrium as a result of their capability to locally consume and convert energy (e.g., generating self-propulsion) [4–8]. Yet, the non-equilibrium nature of this active driving may not always be visible or detectable in the emergent dynamical behavior of active particles, in particular when the active system is being observed on the level of spatial trajectories without resolving the microscopic processes generating the active self-propulsion. Active matter systems may therefore appear to bear certain equilibrium features despite their underlying non-equilibrium nature. We here have assessed this potential resemblance by quantifying the irreversibility of individual steady-state trajectories of active particles confined within a static one-dimensional trapping potential. This setup excludes the occurrence of net

(particle) currents and of non-equilibrium stationary states sustained by external time-periodic driving forces. Without activity, it corresponds to an equilibrium situation with perfect path-wise reversibility. To study the effect of activity on the (ir)reversibility properties of particle trajectories we focused on the so-called active Ornstein-Uhlenbeck particle (AOUP) as a “minimal”, but popular and successful model for active Brownian motion [8, 10, 11, 21, 28, 31, 38–59]. In the AOUP model, active self-propulsion is represented by a fluctuating colored-noise force (Ornstein-Uhlenbeck process) in the equations of motion [32], see Section 2.

The most immediate effect of activity is to create steady-state distributions within the trapping potential, which are different from the equilibrium Boltzmann distribution (see Fig. 10 for an example), but which do not break any symmetry or carry any net currents. Hence, intuition might have tempted us to expect the one-dimensional steady-state dynamics to be path-wise reversible despite its active non-equilibrium character. Our main results for the AOUP model are two-fold:

On the one hand, all steady-state trajectories are perfectly reversible in a harmonic potential, exactly like in equilibrium. This result was proven analytically in Section 4. It is valid for any trajectory of arbitrary duration and for any values of the system parameters. In particular, it does not play any role whether the activity is weak or strong (controlled by D_a in (1)) or whether the persistence time τ_a of the active driving is short or long. Moreover, steady-state trajectories are reversible in a harmonic potential in arbitrary dimensions, not just in a one-dimensional harmonic trap. Our finding generalizes previous results regarding the reversibility of infinitely long trajectories of a harmonically trapped AOUP [66] to individual, finite-time trajectories and corroborates earlier reports that an AOUP in a potential with vanishing third derivative possesses equilibrium-like properties [11, 28, 35, 55].

On the other hand, AOUP trajectories are irreversible in a quartic potential, even in the steady state. We demonstrated this by evaluating the irreversibility production (20) from numerically simulated trajectories (which are much longer than transient relaxation processes). In a quartic double-well potential (Section 5) we identified the jumps between the potential wells, driven by the active fluctuations, as the main source of irreversibility. For large τ_a , the irreversible nature of the individual particle trajectories is even visible to the naked eye, such that we may quite easily distinguish between trajectories being traced out forward in time versus backward in time. In a quartic single-well potential, irreversibility does not seem to be connected in such an obvious way to a distinct feature of the particle trajectories. Nevertheless, irreversibility production can reach rates comparable to those in the double-well potential. Moreover, in both the quartic single- and double-well potentials, we find the irreversibility production to vanish, and thus the AOUP trajectories to become reversible, for small and large τ_a , in agreement with the fact that in these limits the steady-state AOUP can be mapped to a passive Brownian particle at equilibrium (see Appendix C in [13] for an explicit computation of the $\tau_a \rightarrow 0$ limit at constant D_a for arbitrary potentials).

The associated decrease of the average irreversibility production rate $\langle\sigma\rangle$ with

increasing τ_a is in contrast to the growing deviation of the steady-state distribution from the equilibrium Boltzmann distribution (see Fig. 10). This apparent contradiction (and others [15]) highlights that the non-equilibrium characteristics of the steady state of active matter are complex and subtle, in particular with respect to their analogy to the equilibrium state. Different hallmarks of equilibrium (Boltzmann distribution vs. path-wise reversibility vs. violations of Einstein relation etc.) may capture different aspects of this analogy. Concerning the log ratio of path probabilities $\Delta\Sigma$, we would like to emphasize here that—by construction—it does not measure entropy production in the thermal environment and does not quantify departure from equilibrium in that sense. In any model for active matter which simply represents activity by an “effective active force” (like the AOUP model) the entropy production and the corresponding departure from equilibrium due to the microscopic dissipative processes generating the active self-propulsion drive cannot be captured (see also the detailed discussion in [13], and [76] for an explicit model quantifying this microscopic entropy production). Rather, $\Delta\Sigma$ assesses, in the very sense of its definition (6), how irreversible spatial AOUP trajectories are and how closely the AOUP dynamics resembles the path-wise reversibility properties of equilibrium systems.

As we have seen in the present study, the AOUP dynamics can appear time reversible, and thus equilibrium-like, despite the non-equilibrium character of the active self-propulsion. This result directly extends to other physical situations which are described by our model (1), (2). In particular, the equations of motion (1), (2) are well established to capture essential aspects of the dynamical behavior of a passive tracer particle suspended in a “bath” of active swimmers [10, 13, 40, 41]. It would be interesting to connect our findings to the thermodynamic (-like) properties of active matter [77], for instance, by unravelling how the (ir)reversibility of active particle trajectories is related to the active pressure [18, 78] or to motility-induced phase separation [79]. Moreover, analogous studies should be carried out for other models of active Brownian motion, like active Brownian particles or run-and-tumble particles [4].

Acknowledgments

LD acknowledges funding by the Deutsche Forschungsgemeinschaft (DFG) within the Research Unit FOR 2692 under Grant No. 397303734 and by a Nordita Visiting PhD Student Fellowship. SB wishes to thank Frank Jülicher, Charlie Duclut and Joris Pajmians for inspiring discussions. RE acknowledges funding by the Swedish Research Council (Vetenskapsrådet) under the Grants No. 2016-05412. This work was supported by the Paderborn Center for Parallel Computing (PC²) within the Project “hpc-prf-ubinmpt”.

Appendix A. Calculation of $\Gamma_{\text{HP}}(t, t')$

In eq. (12) the explicit form of the “memory kernel” $\Gamma_{\text{HP}}(t, t')$ in the path integral (13) is given for the case of an AOUP being trapped in a harmonic potential. As mentioned in the main text, it turns up as the operator inverse $\int_0^\tau dt' V_{\text{HP}}(t, t') \Gamma_{\text{HP}}(t', t'') = \delta(t - t'')$ of the differential operator

$$V_{\text{HP}}(t, t') = \delta(t - t') \left[-\tau_a^2 \partial_{t'}^2 + 1 + \frac{D_a}{D} + \delta(t') (-\tau_a^2 \partial_{t'} - \tau_a + \bar{C}_{22}) + \delta(\tau - t') (\tau_a^2 \partial_{t'} + \tau_a) \right] \quad (\text{A.1})$$

when performing the Gaussian integral over all realizations $\bar{\eta}$ of the active fluctuations. Since the operator $V_{\text{HP}}(t, t')$ is “diagonal” in its time arguments, the integro-differential equation determining $\Gamma_{\text{HP}}(t, t')$ simplifies to the differential equation

$$\left[-\tau_a^2 \partial_t^2 + 1 + \frac{D_a}{D} + \delta(t) (-\tau_a^2 \partial_t - \tau_a + \bar{C}_{22}) + \delta(\tau - t) (\tau_a^2 \partial_t + \tau_a) \right] \Gamma_{\text{HP}}(t, t') = \delta(t - t'). \quad (\text{A.2})$$

Similar equations have been solved in the Appendices of [13, 16], investigating setups for AOUPs with initial conditions different from the stationary state in a harmonic trap considered here. The mathematical procedure for finding the solution of (A.2) is essentially the same as in [13, 16]. In fact, the differential equation (36) studied in the Appendix of [16] is identical to our (A.2) here when identifying $1/\sigma^2$ with \bar{C}_{22} . We can therefore read off $\Gamma_{\text{HP}}(t, t')$ directly from the solution (17) in [16] by setting $\sigma^2 = 1/\bar{C}_{22}$.

For the sake of completeness, we here briefly repeat the main ideas and a few central steps of the calculation. Exploiting that (A.2) is a linear differential equation we compose $\Gamma_{\text{HP}}(t, t')$ from two parts, $\Gamma_{\text{HP}}(t, t') = G(t, t') + H(t, t')$. The first part is the Green’s function of the inhomogeneous equation $[-\tau_a^2 \partial_t^2 + (1 + D_a/D)]G(t, t') = \delta(t - t')$ with homogeneous boundary conditions $G(0, t') = G(\tau, t') = 0$, the second part solves the homogeneous problem $[-\tau_a^2 \partial_t^2 + (1 + D_a/D)]H(t, t') = 0$ such that the boundary terms are fixed as prescribed by (A.2). We construct both parts, $G(t, t')$ and $H(t, t')$, from the general solution

$$\Gamma(t) = a^+ e^{\lambda t} + a^- e^{-\lambda t}, \quad \lambda = \frac{1}{\tau_a} \sqrt{1 + \frac{D_a}{D}}, \quad a^\pm = \text{const} \quad (\text{A.3})$$

of the homogeneous ordinary differential equation

$$\left[-\tau_a^2 \partial_t^2 + 1 + \frac{D_a}{D} \right] \Gamma(t) = 0 \quad (\text{A.4})$$

associated with (A.2).

For $G(t, t')$, two such solutions, one for $0 < t < t'$ and one for $t' < t < \tau$, are matched at $t = t'$ such that the $\delta(t - t')$ -inhomogeneity appears when evaluating $[-\tau_a^2 \partial_t^2 + (1 + D_a/D)]G(t, t')$. The corresponding matching conditions at $t = t'$ and the homogeneous boundary conditions $G(0, t') = G(\tau, t') = 0$ fix the two sets of parameters a^\pm from the ansatz (A.3) (one set for $0 < t < t'$ and one for $t' < t < \tau$) [13]. Via

these matching conditions at $t = t'$, the time point t' enters the solution $G(t, t')$; it is otherwise a fixed parameter in the differential equations for $G(t, t')$ and $H(t, t')$, just like D , D_a , τ_a and \bar{C}_{22} .

For the function $H(t, t')$, we again make an ansatz of the form (A.3). We fix the coefficients a^\pm by ensuring that the full solution $\Gamma_{\text{HP}}(t, t') = G(t, t') + H(t, t')$ with the Green's function $G(t, t')$ already known from the previous step of the calculation fulfills (A.2). Plugging $G(t, t') + H(t, t')$ into (A.2), and using $[-\tau_a^2 \partial_t^2 + (1 + D_a/D)]G(t, t') = \delta(t - t')$ and $[-\tau_a^2 \partial_t^2 + (1 + D_a/D)]H(t, t') = 0$, we are left with the boundary contributions proportional to $\delta(t)$ and $\delta(\tau - t)$ on the left-hand side of (A.2) (expressed in terms of derivatives of $G(t, t')$, the various system parameters, and the unknowns a^\pm) and with zero on the right-hand side of (A.2). Requiring that each of these boundary contributions vanishes, we obtain a^\pm for the function $H(t, t')$. Finally, the sought solution $\Gamma_{\text{HP}}(t, t')$ is obtained according to the superposition $\Gamma_{\text{HP}}(t, t') = G(t, t') + H(t, t')$.

Appendix B. Reversibility in the harmonic potential

The goal is to show that $\Delta\Sigma[\bar{x}]$ as given in (16) is identically zero. We start by moving the time-derivatives within the integrals from \dot{x}_t and $\dot{x}_{t'}$ to $\Gamma_{\text{HP}}(t, t')$ via partial integration and by sorting the resulting expression for $\Delta\Sigma[\bar{x}]$ into contributions containing genuine double time integrals, single time integrals and pure boundary terms,

$$\frac{\Delta\Sigma[\bar{x}]}{k_B} = \frac{1}{2} \int_0^\tau \int_0^\tau \dagger' x_t K_2(t, t') x_{t'} + \frac{1}{2} \int_0^\tau \dagger x_t [K_\tau(t) x_\tau - K_0(t) x_0] + \frac{1}{2} K(x_\tau^2 - x_0^2), \quad (\text{B.1})$$

with

$$K_2(t, t') = \frac{D_a}{2D^2} \left[-\frac{4k_2}{\gamma} \bar{\Gamma}_{\text{HP}}^{(1,0)}(t, t') + \left(\frac{k_2}{\gamma} \right)^2 \Delta\Gamma_{\text{HP}}(t, t') + \Delta\Gamma_{\text{HP}}^{(1,1)}(t, t') \right], \quad (\text{B.2})$$

$$\begin{aligned} K_\tau(t) &= \frac{D_a}{2D^2} \left[\frac{4k_2}{\gamma} \bar{\Gamma}_{\text{HP}}(t, \tau) - 2\Delta\Gamma_{\text{HP}}^{(1,0)}(t, \tau) \right] \\ &\quad + \frac{\sqrt{2D_a}}{D} \bar{C}_{12} \left[\frac{k_2}{\gamma} \Gamma_{\text{HP}}(\tau - t, 0) - \Gamma_{\text{HP}}^{(1,0)}(\tau - t, 0) \right], \end{aligned} \quad (\text{B.3})$$

$$\begin{aligned} K_0(t) &= \frac{D_a}{2D^2} \left[\frac{4k_2}{\gamma} \bar{\Gamma}_{\text{HP}}(t, 0) - 2\Delta\Gamma_{\text{HP}}^{(1,0)}(t, 0) \right] \\ &\quad + \frac{\sqrt{2D_a}}{D} \bar{C}_{12} \left[\frac{k_2}{\gamma} \Gamma_{\text{HP}}(t, 0) - \Gamma_{\text{HP}}^{(1,0)}(t, 0) \right], \end{aligned} \quad (\text{B.4})$$

$$K = \bar{C}_{11} - \left(\bar{C}_{12}^2 + \frac{\sqrt{2D_a}}{D} \bar{C}_{12} \right) \Gamma_{\text{HP}}(0, 0) - \frac{D_a}{2D^2} \Delta\Gamma_{\text{HP}}(0, 0) - \frac{1}{D} \frac{k_2}{\gamma}, \quad (\text{B.5})$$

where we recall that $\bar{\Gamma}_{\text{HP}} = \frac{1}{2} [\Gamma_{\text{HP}}(t, t') + \Gamma_{\text{HP}}(\tau - t, \tau - t')]$ and $\Delta\Gamma_{\text{HP}} = \Gamma_{\text{HP}}(t, t') - \Gamma_{\text{HP}}(\tau - t, \tau - t')$, as defined below eq. (16). To find these expressions we have exploited $\Delta\Gamma_{\text{HP}}(0, \tau) = \Delta\Gamma_{\text{HP}}(\tau, 0) = 0$, $\Delta\Gamma_{\text{HP}}(\tau, \tau) = -\Delta\Gamma_{\text{HP}}(0, 0)$, and we have used the symmetry $\Gamma_{\text{HP}}(t, t') = \Gamma_{\text{HP}}(t', t)$, implying, e.g., $\Gamma_{\text{HP}}(\tau, t') = \Gamma_{\text{HP}}(t', \tau)$. Moreover, we have introduced the notation $\Gamma_{\text{HP}}^{(i,j)}(t, t')$ to denote the i -th derivative of $\Gamma_{\text{HP}}(t, t')$ with respect to its first argument and the j -th derivative with respect to its second argument, an explicit example being $\Gamma_{\text{HP}}^{(1,0)}(\tau - t, 0) = \frac{\partial \Gamma_{\text{HP}}(t, t')}{\partial t} \Big|_{t=\tau-t, t'=0} = \frac{\partial \Gamma_{\text{HP}}(\tau-t, 0)}{\partial(\tau-t)} = -\frac{\partial \Gamma_{\text{HP}}(\tau-t, 0)}{\partial t}$. Note that the contribution K contains the $\delta(t - t')$ -integral from (16) as a boundary term. In the following we consider the four contributions (B.2)-(B.5) separately.

For convenience we briefly recall some central quantities. We start with the abbreviations from (15),

$$\begin{aligned} \kappa_{\pm\pm} &= \kappa_{\pm} \left(1 - \kappa_{\pm} \tau_a / \bar{C}_{22} \right) \\ &= \kappa_{\pm} \left(1 - \kappa_{\pm} \frac{D + D_a \rho^2}{2(D + D_a \rho)} \right) \\ &= (1 \pm \lambda \tau_a) \left[1 - (1 \pm \lambda \tau_a) \frac{D + D_a \rho^2}{2(D + D_a \rho)} \right] \\ &= \left(1 \pm \sqrt{1 + D_a/D} \right) \left[1 - \left(1 \pm \sqrt{1 + D_a/D} \right) \frac{D + D_a \rho^2}{2(D + D_a \rho)} \right], \end{aligned} \quad (\text{B.6})$$

where in the second line we have used the explicit form of \bar{C}_{22} from (11), and in the third line the definition of $\kappa_{\pm} = 1 \pm \lambda \tau_a = 1 \pm \sqrt{1 + D_a/D}$ given in eq. (15). Some combinations of these constants, which we will need in the following calculations, are

$$\kappa_{++} + \kappa_{--} = -\tau_a^2 \left[(k_2/\gamma)^2 + \lambda^2 \right] \frac{D_a \rho^2}{D + D_a \rho}, \quad (\text{B.7})$$

$$\kappa_{++} - \kappa_{--} = \tau_a^2 (2k_2 \lambda / \gamma) \frac{D_a \rho^2}{D + D_a \rho}, \quad (\text{B.8})$$

$$\begin{aligned} \kappa_{+-} - \kappa_{++} &= -\frac{1}{2} (\lambda \tau_a + 1) (\kappa_{++} - \kappa_{--} - 2\lambda \tau_a) \\ &= \lambda \tau_a (\lambda \tau_a + 1) \frac{D + D_a \rho^2}{D + D_a \rho}, \end{aligned} \quad (\text{B.9})$$

$$\begin{aligned} \kappa_{-+} - \kappa_{--} &= -\frac{1}{2} (\lambda \tau_a - 1) (\kappa_{++} - \kappa_{--} - 2\lambda \tau_a) \\ &= \lambda \tau_a (\lambda \tau_a - 1) \frac{D + D_a \rho^2}{D + D_a \rho}. \end{aligned} \quad (\text{B.10})$$

We also recall the explicit form of the integral kernel $\Gamma_{\text{HP}}(t, t')$ from (14),

$$\Gamma_{\text{HP}}(t, t') = \frac{\kappa_{+-} e^{-\lambda|t-t'|} + \kappa_{-+} e^{-\lambda(2\tau-|t-t'|)} - \kappa_{++} e^{-\lambda(t+t')} - \kappa_{--} e^{-\lambda(2\tau-t-t')}}{2\tau_a^2 \lambda (\kappa_{+-} - \kappa_{-+} e^{-2\lambda\tau})}, \quad (\text{B.11})$$

and the definitions $\bar{\Gamma}_{\text{HP}} = \frac{1}{2} [\Gamma_{\text{HP}}(t, t') + \Gamma_{\text{HP}}(\tau - t, \tau - t')]$ and $\Delta\Gamma_{\text{HP}} = \Gamma_{\text{HP}}(t, t') - \Gamma_{\text{HP}}(\tau - t, \tau - t')$.

We can now compute the various combinations and derivatives of $\Gamma_{\text{HP}}(t, t')$ appearing in (B.2),

$$\bar{\Gamma}_{\text{HP}}^{(1,0)}(t, t') = \frac{\lambda \text{sign}(t' - t) [\kappa_{+-} e^{-\lambda|t-t'|} - \kappa_{-+} e^{-\lambda(2\tau-|t-t'|)}]}{2\tau_a^2 \lambda (\kappa_{+-} - \kappa_{-+} e^{-2\lambda\tau})} - \frac{\frac{\lambda}{2} (\kappa_{++} + \kappa_{--}) [e^{-\lambda(2\tau-t-t')} - e^{-\lambda(t+t')}] }{2\tau_a^2 \lambda (\kappa_{+-} - \kappa_{-+} e^{-2\lambda\tau})}, \quad (\text{B.12})$$

$$\Delta\Gamma_{\text{HP}}(t, t') = \frac{(\kappa_{++} - \kappa_{--}) [e^{-\lambda(2\tau-t-t')} - e^{-\lambda(t+t')}] }{2\tau_a^2 \lambda (\kappa_{+-} - \kappa_{-+} e^{-2\lambda\tau})}, \quad (\text{B.13})$$

$$\Delta\Gamma_{\text{HP}}^{(1,1)}(t, t') = \lambda^2 \Delta\Gamma_{\text{HP}}(t, t'). \quad (\text{B.14})$$

The first line in (B.12) is an odd function upon exchange of t and t' and therefore does not contribute to the double integral in (B.1). The remaining terms in $K_2(t, t')$ are proportional to $[(2k_2\lambda/\gamma)(\kappa_{++} + \kappa_{--}) + [(k_2/\gamma)^2 + \lambda^2](\kappa_{++} - \kappa_{--})] [e^{-\lambda(2\tau-t-t')} - e^{-\lambda(t+t')}]$. With (B.7) and (B.8) we see that these terms are zero as well.

Next, we consider $K_\tau(t)$, see eq. (B.3). The expressions involving $\Gamma_{\text{HP}}(t, t')$ read

$$\bar{\Gamma}_{\text{HP}}(t, \tau) = \frac{[\kappa_{+-} - \frac{1}{2}(\kappa_{++} + \kappa_{--})] e^{-\lambda(\tau-t)} + [\kappa_{-+} - \frac{1}{2}(\kappa_{++} + \kappa_{--})] e^{-\lambda(\tau+t)}}{2\tau_a^2 \lambda (\kappa_{+-} - \kappa_{-+} e^{-2\lambda\tau})}, \quad (\text{B.15})$$

$$\Delta\Gamma_{\text{HP}}^{(1,0)}(t, \tau) = \frac{\lambda(\kappa_{++} - \kappa_{--}) [e^{-\lambda(\tau-t)} + e^{-\lambda(\tau+t)}]}{2\tau_a^2 \lambda (\kappa_{+-} - \kappa_{-+} e^{-2\lambda\tau})}, \quad (\text{B.16})$$

$$\Gamma_{\text{HP}}(\tau - t, 0) = \frac{(\kappa_{+-} - \kappa_{++}) e^{-\lambda(\tau-t)} + (\kappa_{-+} - \kappa_{--}) e^{-\lambda(\tau+t)}}{2\tau_a^2 \lambda (\kappa_{+-} - \kappa_{-+} e^{-2\lambda\tau})}, \quad (\text{B.17})$$

$$\Gamma_{\text{HP}}^{(1,0)}(\tau - t, 0) = \frac{-\lambda(\kappa_{+-} - \kappa_{++}) e^{-\lambda(\tau-t)} + \lambda(\kappa_{-+} - \kappa_{--}) e^{-\lambda(\tau+t)}}{2\tau_a^2 \lambda (\kappa_{+-} - \kappa_{-+} e^{-2\lambda\tau})}. \quad (\text{B.18})$$

Plugging them into (B.3), using $\bar{C}_{12} = -\sqrt{2D_a} \frac{k_2\tau_a}{\gamma} \rho / (D + D_a\rho^2)$ (see (11)), and skipping common t -independent factors, we find

$$\begin{aligned} K_\tau(t) \propto & \left\{ \frac{2k_2\tau_a}{\gamma} \left[\kappa_{+-} - \kappa_{++} + \frac{1}{2}(\kappa_{++} - \kappa_{--}) \right] - \lambda\tau_a(\kappa_{++} - \kappa_{--}) \right. \\ & \left. - \frac{2D\rho}{D + D_a\rho^2} \frac{k_2\tau_a}{\gamma} \left(\frac{k_2\tau_a}{\gamma} + \lambda\tau_a \right) (\kappa_{+-} - \kappa_{++}) \right\} e^{-\lambda(\tau-t)} \\ & + \left\{ \frac{2k_2\tau_a}{\gamma} \left[\kappa_{-+} - \kappa_{--} - \frac{1}{2}(\kappa_{++} - \kappa_{--}) \right] - \lambda\tau_a(\kappa_{++} - \kappa_{--}) \right. \\ & \left. - \frac{2D\rho}{D + D_a\rho^2} \frac{k_2\tau_a}{\gamma} \left(\frac{k_2\tau_a}{\gamma} - \lambda\tau_a \right) (\kappa_{-+} - \kappa_{--}) \right\} e^{-\lambda(\tau+t)} \end{aligned} \quad (\text{B.19})$$

Using (B.8), (B.9), (B.10), and keeping in mind that $1/\rho = 1 + k_2\tau_a/\gamma$ and $D_a/D = (\lambda\tau_a)^2 - 1$, we recognize that the expressions in curly brackets in front of $e^{-\lambda(\tau-t)}$ and $e^{-\lambda(\tau+t)}$ both vanish, such that we conclude $K_\tau(t) = 0$. By a completely analogous calculation we can show that $K_0(t) = 0$ as well (cf. (B.4)).

We finally turn to K , eq. (B.5). With the expressions for \bar{C}_{11} and \bar{C}_{12} from (11), we can simplify $\bar{C}_{11} - k_2/(D\gamma) = [k_2/(D\gamma)] \frac{-D_a \rho^2}{D+D_a \rho^2}$ and $\bar{C}_{12}^2 + (\sqrt{2D_a}/D)\bar{C}_{12} = 2\tau_a[k_2/(D\gamma)] \frac{-D_a \rho^2}{D+D_a \rho^2} \frac{D+D_a \rho}{D+D_a \rho^2}$. Then, using

$$\Gamma_{\text{HP}}(0,0) = \frac{(\kappa_{+-} - \kappa_{++}) + (\kappa_{-+} - \kappa_{--}) e^{-2\lambda\tau}}{2\tau_a^2 \lambda (\kappa_{+-} - \kappa_{-+} e^{-2\lambda\tau})}, \quad (\text{B.20})$$

$$\Delta\Gamma_{\text{HP}}(0,0) = \frac{(\kappa_{++} - \kappa_{--}) (e^{-2\lambda\tau} - 1)}{2\tau_a^2 \lambda (\kappa_{+-} - \kappa_{-+} e^{-2\lambda\tau})}, \quad (\text{B.21})$$

and eqs. (B.8), (B.9), (B.10), we rewrite K as

$$\begin{aligned} K &= \frac{k_2}{D\gamma} \frac{-D_a \rho^2}{D+D_a \rho^2} \left[1 - \frac{(\lambda\tau_a + 1) + (\lambda\tau_a - 1) e^{-2\lambda\tau}}{\kappa_{+-} - \kappa_{-+} e^{-2\lambda\tau}} \right. \\ &\quad \left. + \frac{D_a}{D} \frac{D+D_a \rho^2}{2(D+D_a \rho)} \frac{e^{-2\lambda\tau} - 1}{\kappa_{+-} - \kappa_{-+} e^{-2\lambda\tau}} \right] \\ &= \frac{k_2}{D\gamma} \frac{-D_a \rho^2}{D+D_a \rho^2} \left\{ 1 - \left[1 + \lambda\tau_a + \frac{D_a}{D} \frac{D+D_a \rho^2}{2(D+D_a \rho)} \right] \frac{1}{\kappa_{+-} - \kappa_{-+} e^{-2\lambda\tau}} \right. \\ &\quad \left. + \left[1 - \lambda\tau_a + \frac{D_a}{D} \frac{D+D_a \rho^2}{2(D+D_a \rho)} \right] \frac{e^{-2\lambda\tau}}{\kappa_{+-} - \kappa_{-+} e^{-2\lambda\tau}} \right\}. \quad (\text{B.22}) \end{aligned}$$

Recalling that $D_a/D = (\lambda\tau_a)^2 - 1 = -(1 - \lambda\tau_a)(1 + \lambda\tau_a)$ and comparing the two terms in the square brackets with (B.6), we can identify the square bracket in the first line as κ_{+-} and the square bracket in the second line as κ_{-+} . We therefore conclude that $K = 0$.

In summary, we hence find that $\Delta\Sigma[\bar{x}]$ given in (16) vanishes identically, as claimed in the main text (see Sec. 4).

References

- [1] Jarzynski C 2011 *Annu. Rev. Condens. Matter Phys.* **2** 7.1–7.23
- [2] Seifert U 2012 *Rep. Prog. Phys.* **75** 126001 URL <http://stacks.iop.org/0034-4885/75/i=12/a=126001>
- [3] Seifert U 2005 *Phys. Rev. Lett.* **95** 040602
- [4] Romanczuk P, Bär M, Ebeling W, Lindner B and Schimansky-Geier L 2012 *The European Physical Journal Special Topics* **202** 1–162
- [5] Elgeti J, Winkler R G and Gompper G 2015 *Rep. Prog. Phys.* **78** 056601
- [6] Bechinger C, Di Leonardo R, Löwen H, Reichhardt C, Volpe G and Volpe G 2016 *Rev. Mod. Phys.* **88**(4) 045006 URL <https://link.aps.org/doi/10.1103/RevModPhys.88.045006>
- [7] Ramaswamy S 2017 *J. Stat. Mech: Theory Exp.* **2017** 054002
- [8] Fodor É and Marchetti M C 2018 *Physica A* **504** 106–120
- [9] Aranson I S 2013 *Phys. Usp.* **56** 79

- [10] Argun A, Moradi A R, Pınar E, Bağcı G B, Imparato A and Volpe G 2016 *Phys. Rev. E* **94**(6) 062150 URL <https://link.aps.org/doi/10.1103/PhysRevE.94.062150>
- [11] Fodor E, Nardini C, Cates M E, Tailleur J, Visco P and van Wijland F 2016 *Phys. Rev. Lett.* **117**(3) 038103 URL <http://link.aps.org/doi/10.1103/PhysRevLett.117.038103>
- [12] Nardini C, Fodor É, Tjhung E, van Wijland F, Tailleur J and Cates M E 2017 *Phys. Rev. X* **7** 021007
- [13] Dabelow L, Bo S and Eichhorn R 2019 *Phys. Rev. X* **9** 021009
- [14] Caprini L, Marconi U M B, Puglisi A and Vulpiani A 2019 *J. Stat. Mech: Theory Exp.* **2019** 053203
- [15] Flenner E and Szamel G 2020 *Phys. Rev. E* **102** 022607
- [16] Dabelow L and Eichhorn R 2021 *Front. Phys.* **8** 516
- [17] Ginot F, Theurkauff I, Levis D, Ybert C, Bocquet L, Berthier L and Cottin-Bizonne C 2015 *Phys. Rev. X* **5** 011004
- [18] Solon A P, Stenhammar J, Wittkowski R, Kardar M, Kafri Y, Cates M E and Tailleur J 2015 *Phys. Rev. Lett.* **114** 198301
- [19] Takatori S C and Brady J F 2015 *Phys. Rev. E* **91** 032117
- [20] Preisler Z and Dijkstra M 2016 *Soft Matter* **12** 6043–6048
- [21] Wittmann R, Marconi U M B, Maggi C and Brader J M 2017 *J. Stat. Mech: Theory Exp.* **2017** 113208
- [22] Solon A P, Stenhammar J, Cates M E, Kafri Y and Tailleur J 2018 *Phys. Rev. E* **97** 020602
- [23] Solon A P, Stenhammar J, Cates M E, Kafri Y and Tailleur J 2018 *New J. Phys.* **20** 075001
- [24] Paliwal S, Rodenburg J, van Roij R and Dijkstra M 2018 *New J. Phys.* **20** 015003
- [25] Pietzonka P, Fodor É, Lohrmann C, Cates M E and Seifert U 2019 *Phys. Rev. X* **9** 041032
- [26] Mandal S, Liebchen B and Löwen H 2019 *Phys. Rev. Lett.* **123** 228001
- [27] Crosato E, Prokopenko M and Spinney R E 2019 *Phys. Rev. E* **100** 042613
- [28] Dal Cengio S, Levis D and Pagonabarraga I 2019 *Phys. Rev. Lett.* **123** 238003
- [29] GrandPre T, Klymko K, Mandadapu K K and Limmer D T 2020 *arXiv preprint arXiv:2007.12149*
- [30] Wexler D, Gov N, Rasmussen K Ø and Bel G 2020 *Phys. Rev. Research* **2** 013003
- [31] Fodor É, Nemoto T and Vaikuntanathan S 2020 *New J. Phys.* **22** 013052
- [32] Martin D, O’Byrne J, Cates M E, Fodor É, Nardini C, Tailleur J and van Wijland F 2020 *arXiv preprint arXiv:2008.12972*

- [33] Gardiner C 1985 *Handbook of Stochastic Methods for Physics, Chemistry, and the Natural Sciences* 2nd ed (Springer) 4th reprint, 1997
- [34] Van Kampen N G 1992 *Stochastic processes in physics and chemistry* vol 1 (Elsevier)
- [35] Zamponi F, Bonetto F, Cugliandolo L F and Kurchan J 2005 *J. Stat. Mech.: Theory Exp.* **2005** P09013
- [36] Kubo R 1966 *Rep. Prog. Phys.* **29** 255 URL <http://stacks.iop.org/0034-4885/29/i=1/a=306>
- [37] Marconi U M B, Puglisi A, Rondoni L and Vulpiani A 2008 *Phys. Rep.* **461** 111–195
- [38] Fily Y and Marchetti M C 2012 *Phys. Rev. Lett.* **108**(23) 235702 URL <http://link.aps.org/doi/10.1103/PhysRevLett.108.235702>
- [39] Farage T F F, Krininger P and Brader J M 2015 *Phys. Rev. E* **91**(4) 042310 URL <http://link.aps.org/doi/10.1103/PhysRevE.91.042310>
- [40] Maggi C, Paoluzzi M, Pellicciotta N, Lepore A, Angelani L and Di Leonardo R 2014 *Phys. Rev. Lett.* **113**(23) 238303 URL <http://link.aps.org/doi/10.1103/PhysRevLett.113.238303>
- [41] Maggi C, Paoluzzi M, Angelani L and Di Leonardo R 2017 *Sci. Rep.* **7** 17588
- [42] Marconi U M B, Puglisi A and Maggi C 2017 *Sci. Rep.* **7** 46496
- [43] Mandal D, Klymko K and DeWeese M R 2017 *Phys. Rev. Lett.* **119** 258001
- [44] Puglisi A and Marini Bettolo Marconi U 2017 *Entropy* **19** 356 ISSN 1099-4300 URL <http://dx.doi.org/10.3390/e19070356>
- [45] Koumakis N, Maggi C and Di Leonardo R 2014 *Soft Matter* **10** 5695–5701
- [46] Szamel G 2014 *Phys. Rev. E* **90** 012111
- [47] Szamel G, Flenner E and Berthier L 2015 *Phys. Rev. E* **91** 062304
- [48] Maggi C, Marconi U M B, Gnan N and Di Leonardo R 2015 *Sci. Rep.* **5** 10742
- [49] Flenner E, Szamel G and Berthier L 2016 *Soft Matter* **12**(34) 7136–7149 URL <http://dx.doi.org/10.1039/C6SM01322H>
- [50] Paoluzzi M, Maggi C, Marini Bettolo Marconi U and Gnan N 2016 *Phys. Rev. E* **94** 052602
- [51] Marini Bettolo Marconi U, Gnan N, Paoluzzi M, Maggi C and Di Leonardo R 2016 *Sci. Rep.* **6** 23297 URL <http://dx.doi.org/10.1038/srep23297>
- [52] Szamel G 2017 *EPL (Europhysics Letters)* **117** 50010
- [53] Sandford C, Grosberg A Y and Joanny J F 2017 *Phys. Rev. E* **96** 052605
- [54] Caprini L, Marconi U M B and Vulpiani A 2018 *J. Stat. Mech.: Theory Exp.* **2018** 033203
- [55] Bonilla L 2019 *Phys. Rev. E* **100** 022601
- [56] Woillez E, Kafri Y and Lecomte V 2020 *J. Stat. Mech.: Theory Exp.* **2020** 063204
- [57] Berthier L and Kurchan J 2013 *Nat. Phys.* **9** 310–314

- [58] Marini Bettolo Marconi U and Maggi C 2015 *Soft Matter* **11**(45) 8768–8781 URL <http://dx.doi.org/10.1039/C5SM01718A>
- [59] Shankar S and Marchetti M C 2018 *Phys. Rev. E* **98** 020604
- [60] Onsager L and Machlup S 1953 *Phys. Rev.* **91**(6) 1505–1512 URL <http://link.aps.org/doi/10.1103/PhysRev.91.1505>
- [61] Machlup S and Onsager L 1953 *Phys. Rev.* **91**(6) 1512–1515 URL <http://link.aps.org/doi/10.1103/PhysRev.91.1512>
- [62] Cugliandolo L F and Lecomte V 2017 *J. Phys. A: Math. Theor.* **50** 345001
- [63] Seifert U 2018 *Physica A* **504** 176–191
- [64] Roldán É, Neri I, Dörpinghaus M, Meyr H and Jülicher F 2015 *Phys. Rev. Lett.* **115** 250602
- [65] Risken H 1984 *The Fokker-Planck Equation* (Springer)
- [66] Dadhichi L P, Maitra A and Ramaswamy S 2018 *Journal of Statistical Mechanics: Theory and Experiment* **2018** 123201
- [67] Volpe G and Petrov D 2006 *Phys. Rev. Lett.* **97** 210603
- [68] Volpe G, Volpe G and Petrov D 2007 *Phys. Rev. E* **76** 061118
- [69] Filliger R and Reimann P 2007 *Phys. Rev. Lett.* **99**(23) 230602 URL <http://link.aps.org/doi/10.1103/PhysRevLett.99.230602>
- [70] Chiang K H, Lee C L, Lai P Y and Chen Y F 2017 *Phys. Rev. E* **96** 032123
- [71] Argun A, Soni J, Dabelow L, Bo S, Pesce G, Eichhorn R and Volpe G 2017 *Phys. Rev. E* **96** 052106
- [72] Cerasoli S, Dotsenko V, Oshanin G and Rondoni L 2018 *Phys. Rev. E* **98** 042149
- [73] Pietzonka P and Seifert U 2018 *Phys. Rev. Lett.* **120** 190602
- [74] Fily Y 2019 *The Journal of Chemical Physics* **150** 174906
- [75] Caprini L, Marini Bettolo Marconi U, Puglisi A and Vulpiani A 2019 *The Journal of Chemical Physics* **150** 024902
- [76] Pietzonka P and Seifert U 2018 *J. Phys. A: Math. Theor.* **51** 01LT01
- [77] Takatori S C and Brady J F 2016 *Current Opinion in Colloid & Interface Science* **21** 24–33
- [78] Takatori S C, Yan W and Brady J F 2014 *Phys. Rev. Lett.* **113** 028103
- [79] Cates M E and Tailleur J 2015 *Annual Review of Condensed Matter Physics* **6** 219–244 (Preprint <https://doi.org/10.1146/annurev-conmatphys-031214-014710>) URL <https://doi.org/10.1146/annurev-conmatphys-031214-014710>